

# Lighting the Darkness in the Deep Learning Era

Chongyi Li, Chunle Guo, Linghao Han, Jun Jiang, Ming-Ming Cheng, *Senior Member, IEEE*,  
Jinwei Gu, *Senior Member, IEEE*, and Chen Change Loy, *Senior Member, IEEE*

**Abstract**— Low-light image enhancement (LLIE) aims at improving the perception or interpretability of an image captured in an environment with poor illumination. Recent advances in this area are dominated by deep learning-based solutions, where many learning strategies, network structures, loss functions, training data, etc. have been employed. In this paper, we provide a comprehensive survey to cover various aspects ranging from algorithm taxonomy to unsolved open issues. To examine the generalization of existing methods, we propose a large-scale low-light image and video dataset, in which the images and videos are taken by different mobile phones' cameras under diverse illumination conditions. Besides, for the first time, we provide a unified online platform that covers many popular LLIE methods, of which the results can be produced through a user-friendly web interface. In addition to qualitative and quantitative evaluation of existing methods on publicly available and our proposed datasets, we also validate their performance in face detection in the dark. This survey together with the proposed dataset and online platform could serve as a reference source for future study and promote the development of this research field. The proposed platform and the collected methods, datasets, and evaluation metrics are publicly available and will be regularly updated at <https://github.com/Li-Chongyi/Lighting-the-Darkness-in-the-Deep-Learning-Era-Open>. We will release our low-light image and video dataset.

**Index Terms**—Low-light image and video enhancement, image and video restoration, computational photography, survey.

## 1 INTRODUCTION

IMAGES are often taken under sub-optimal lighting conditions, under the influence of back-lit, non-uniform illumination and weak lighting, due to inevitable environmental and/or technical constraints such as insufficient illumination and limited exposure time. Such images suffer from the compromised aesthetic quality and unsatisfactory transmission of information for high-level tasks such as object tracking, recognition and detection. Figure 1 shows some examples of the degradations induced by sub-optimal lighting conditions.

Low-light enhancement is one of the fundamental tasks in image processing. It enjoys a wide range of applications in different areas, including visual surveillance, autonomous driving, and computational photography. In particular, smartphone photography has become ubiquitous and prominent. Limited by the size of camera aperture, the requirement of real-time processing, and the constraint of memory, taking photographs with a smartphone's camera in a dim environment is especially challenging. There is an exciting research arena of enhancing low-light images and videos in such applications.

Traditional methods for low-light enhancement include Histogram Equalization-based methods [28], [29] and Retinex model-based methods [30], [31], [32], [33], [34], [35], [36], [37]. The latter received relatively more attention. A typical Retinex model-based approach decomposes a low-light image into a reflection component and an illumination



Fig. 1: Examples of images taken under sub-optimal lighting conditions. These images suffer from the buried scene content, reduced contrast, boosted noise, and inaccurate color.

component by some kind of prior or regularization. The estimated reflection component is treated as the enhanced result. Such methods have some limitations: **1)** the ideal assumption that treats the reflection component as the enhanced result does not always hold, especially given various

C. Li and C. C. Loy are with the S-Lab, Nanyang Technological University (NTU), Singapore (e-mail: chongyi.li@ntu.edu.sg and ccloy@ntu.edu.sg).  
C. Guo, L. Han, and M. M. Cheng are with the College of Computer Science, Nankai University, Tianjin, China (e-mail: guochunle@nankai.edu.cn, llhan@mail.nankai.edu.cn, and cmm@nankai.edu.cn).  
J. Jiang and J. Gu are with the SenseTime (e-mail: jiangjun@sensebrain.site and gujinwei@sensebrain.site).  
C. Li and C. Guo contribute equally.  
C. C. Loy is the corresponding author.

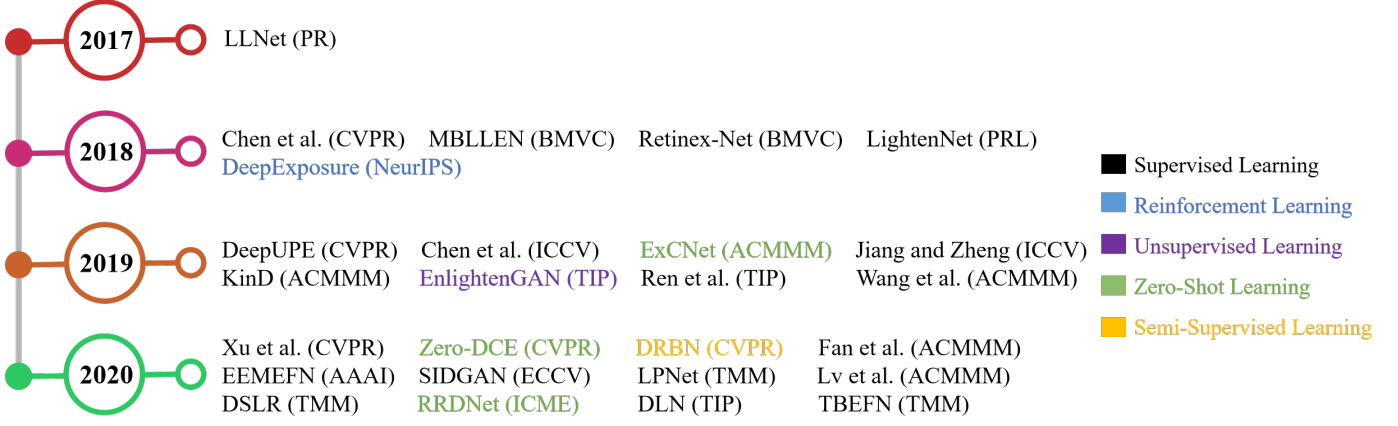


Fig. 2: A concise milestone of deep learning-based low-light image and video enhancement methods. Supervised learning-based methods: LLNet [1], Chen et al. [2], MBLLEN [3], Retinex-Net [4], LightenNet [5], SCIE [6], DeepUPE [7], Chen et al. [8], Jiang and Zheng [9], Wang et al. [10], KinD [11], Ren et al. [12], Xu et al. [13], Fan et al. [14], Lv et al. [15], EEMEFN [16], SIDGAN. [17], LPNet [18], DLN [19], TBEFN [20], and DSLR [21]. Reinforcement learning-based method: DeepExposure [22]. Unsupervised learning-based method: EnlightenGAN [23]. Zero-shot learning-based methods: ExCNet [24], Zero-DCE [25], and RRDNet [26]. Semi-supervised learning-based method: DRBN [27].

illumination properties, which could lead to unrealistic enhancement such as loss of details and distorted colors, 2) the noise is usually ignored in the Retinex model, thus it is remained or amplified in the enhanced results, 3) finding an effective prior or regularization is challenging. Inaccurate prior or regularization may result in artifacts and color deviations in the enhanced results, and 4) the runtime is relatively long because of their complicated optimization process.

Recent years have witnessed the compelling success of deep learning-based LLIE since the first seminal work [1]. Deep learning-based solutions enjoy better accuracy, robustness, and speed over conventional methods, thus attracting increasing attention in recent years. A concise milestone of deep learning-based LLIE methods is shown in Figure 2. As shown, since 2017, the number of deep learning-based solutions has grown year by year. Learning strategies used in these solutions cover Supervised Learning (SL), Reinforcement Learning (RL), Unsupervised Learning (UL), Zero-Shot Learning (ZSL), and Semi-Supervised Learning (SSL). Note that we only report some representative methods in Figure 2. In fact, there are more than 100 papers on deep learning-based methods from 2017 to 2020, more than the total number of conventional methods. Moreover, although some general photo enhancement methods [38], [39], [40], [41], [42], [43], [44], [45], [46] can improve the brightness of images to some extent, we omit them in this survey as they are not designed to handle diverse low-light conditions. We concentrate on deep learning-based solutions that are specially developed for low-light image and video enhancement.

Despite deep learning has dominated the research of LLIE, an in-depth and comprehensive survey on deep learning-based solutions is lacking. There are two reviews of LLIE [47], [48]. In comparison to [47] that mainly reviews conventional LLIE methods and [48] that explores the experimental performance of several conventional and deep learning-based LLIE methods from the perspective

of both human and machine visions, our survey has the following unique characteristics: 1) Our work is the first to systematically and comprehensively review recent advances of deep learning-based LLIE. We provide in-depth analysis and discussion in various aspects, covering learning strategies, network structures, loss functions, training datasets, testing datasets, evaluation metrics, etc. 2) We propose a large-scale dataset that contains images and videos captured by different devices under diverse illumination conditions to evaluate the generalization of existing methods. Consequently, we offer insights for critical open issues, challenges, and future directions. Moreover, we are the first, to the best of our knowledge, to compare the performance of LLIE methods on low-light videos captured in diverse real-world scenes. 3) We provide an online platform that covers many popular deep learning-based LLIE methods, where the results can be produced by a user-friendly web interface. This unified platform solves the issues of comparing different methods that are implemented in different deep learning platforms and require different hardware configurations. With our platform, one without any GPUs can assess the results of different methods for any input images online.

We hope that our survey could provide novel insights and inspiration to facilitate the understanding of deep learning-based LLIE, foster research on the raised open issues, and speed up the development of this research field.

## 2 DEEP LEARNING-BASED LLIE

### 2.1 Problem Definition

We first give a common formulation of the deep learning-based LLIE problem. For a low-light image  $I \in \mathbb{R}^{W \times H \times 3}$  of width  $W$  and height  $H$ , the process can be modeled as:

$$\hat{R} = \mathcal{F}(I; \theta), \quad (1)$$

where  $\hat{R} \in \mathbb{R}^{W \times H \times 3}$  is the enhanced result and  $\mathcal{F}$  represents the network with trainable parameters  $\theta$ . The purpose



of deep learning is to find optimal network parameters  $\hat{\theta}$  that minimizes the error:

$$\hat{\theta} = \underset{\theta}{\operatorname{argmin}} \mathcal{L}(\hat{R}, R), \quad (2)$$

where  $R \in \mathbb{R}^{W \times H \times 3}$  is the ground truth, and the loss function  $\mathcal{L}(\hat{R}, R)$  drives the optimization of network. Various loss functions such as supervised loss and unsupervised loss can be used in the process of network training. More details will be presented in Section 3.

## 2.2 Learning Strategies

According to different learning strategies, we categorize existing LLIE methods into supervised learning, reinforcement learning, unsupervised learning, zero-shot learning, and semi-supervised learning. A statistic analysis from different perspectives is presented in Figure 3. In what follows, we review some representative methods of each strategy.

**Supervised Learning.** For supervised learning-based LLIE methods, they can be further divided into end-to-end methods, deep Retinex-based methods, and realistic data-driven methods.

The first deep learning-based LLIE method LLNet [1] employs a variant of stacked-sparse denoising autoencoder [49] to brighten and denoise low-light images simultaneously. This pioneering work inspires the usage of end-to-end networks in LLIE. Lv et al. [3] propose an end-to-end multi-branch enhancement network (MBLLEN). The MBLLEN improves the performance of LLIE via extracting effective feature representations by a feature extraction module, an enhancement module, and a fusion module. The same authors [15] propose other three subnetworks including an Illumination-Net, a Fusion-Net, and a Restoration-Net to further improve the performance. Ren et al. [12] design a more complex end-to-end network that comprises an encoder-decoder network for image content enhancement and a recurrent neural network for image edge enhancement. Similar to [12], Zhu et al. [16] propose a method called EEMEFN. The EEMEFN consists of two stages: multi-exposure fusion and edge enhancement. A multi-exposure fusion network, TBEFN [20], is proposed for LLIE. The TBEFN estimates a transfer function in two branches, of which two enhancement results can be obtained. At last, a simple average scheme is employed to fuse these two images and further refine the result via a refinement unit. In addition, pyramid network (LPNet) [18], residual network [19], and Laplacian pyramid [21] (DSLR) are introduced into LLIE. These methods learn to effectively and efficiently integrate feature representations via commonly used end-to-end network structures for LLIE. Recently, based on the observation that noise exhibits different levels of contrast in different frequency layers, Xu et al. [50] proposed a frequency-based decomposition-and-enhancement network. This network recovers image contents with noise suppression in the low-frequency layer while inferring the details in the high-frequency layer.

In comparison to directly learning an enhanced result in an end-to-end network, deep Retinex-based methods enjoy better enhancement performance in most cases owing to the physically explicable Retinex theory [51], [52]. Deep

retinex-based methods usually separately enhance the luminance component and the reflectance components via specialized subnetworks. A Retinex-Net is proposed in [4]. The Retinex-Net includes a Decom-Net that splits the input image into light-independent reflectance and structure-aware smooth illumination and an Enhance-Net that adjusts the illumination map for low-light enhancement. To reduce the computational burden, Li et al. [5] propose a lightweight LightenNet for weakly illuminated image enhancement, which only consists of four layers. The LightenNet takes a weakly illuminated image as the input and then estimates its illumination map. Based on the Retinex theory [51], [52], the enhanced image is obtained by dividing the illumination map by the input image. To accurately estimate the illumination map, Wang et al. [53] extract the global and local features to learn an image-to-illumination mapping by their proposed DeepUPE network. Zhang et al. [11] separately develop three subnetworks for layer decomposition, reflectance restoration, and illumination adjustment, called KinD. Furthermore, the authors alleviate the visual defects left in the results of KinD [11] by a multi-scale illumination attention module. The improved KinD is called KinD++ [54]. To solve the issue that the noise is omitted in the deep Retinex-based methods, Wang et al. [10] propose a progressive Retinex network, where an IM-Net estimates the illumination and a NM-Net estimates the noise level. These two subnetworks work in a progressive mechanism until obtaining stable results. Fan et al. [14] integrate semantic segmentation and Retinex model for further improving the enhancement performance in real cases. The core idea is to use semantic prior to guide the enhancement of both the illumination component and the reflectance component.

Although the above-mentioned methods can achieve decent performance, they show poor generalization capability in real low-light cases due to the usage of synthetic training data. To solve this issue, some methods attempt to generate more realistic training data or capture real data. Cai et al. [6] build a multi-exposure image dataset, where the low-contrast images of different exposure levels have their corresponding high-quality reference images. Each high-quality reference image is obtained by subjectively selecting the best output from 13 results enhanced by different methods. Moreover, a frequency decomposition network is trained on the built dataset and separately enhances the high-frequency layer and the low-frequency layer via a two-stage structure. Chen et al. [2] collect a real low-light image dataset (SID) and train the U-Net [55] to learn a mapping from low-light raw data to the corresponding long-exposure high-quality reference image in the sRGB space. Further, Chen et al. [8] extend the SID dataset to low-light videos (DRV). The DRV contains static videos with the corresponding long-exposure ground truths. To ensure the generalization capability of processing the videos of dynamic scenes, a siamese network is proposed. To enhance the moving objects in the dark, Jiang and Zheng [9] design a co-axis optical system to capture temporally synchronized and spatially aligned low-light and well-lighted video pairs (SMOID). Unlike the DRV video dataset [8], the SMOID video dataset contains dynamic scenes. To learn the mapping from raw low-light video to well-lighted video in the sRGB space, a 3D U-Net-based network is proposed. Con-

sidering the limitations of previous low-light video datasets such as DRV dataset [8] only containing statistic videos and SMOID dataset [9] only having 179 video pairs, Triantafyllidou et al. [17] propose a low-light video synthesis pipeline, dubbed SIDGAN. The SIDGAN can produce dynamic video data (RAW-to-RGB) by a semi-supervised dual CycleGAN with intermediate domain mapping. To train this pipeline, the real-world videos are collected from Vimeo-90K dataset [56]. The low-light raw video data and the corresponding long-exposure images are sampled from DRV dataset [8]. With the synthesized training data, this work adopts the same U-Net network structure as [2] for low-light video enhancement.

**Reinforcement Learning.** Without the paired training data, Yu et al. [22] learn to expose photos with reinforcement adversarial learning, named DeepExposure. Specifically, an input image is first segmented into sub-images according to exposures. For each sub-image, a local exposure is learned by the policy network sequentially based on reinforcement learning. The reward evaluation function is approximated by adversarial learning. At last, each local exposure is employed to retouch the input, thus obtaining multiple retouched images under different exposures. The final result is achieved by fusing these images.

**Unsupervised Learning.** Training a deep model on paired data may result in overfitting and limited generalization capability. To solve this issue, an unsupervised learning method named EnlighenGAN is proposed in [23]. The EnlighenGAN adopts an attention-guided U-Net [55] as the generator and uses the global-local discriminators to ensure the enhanced results look like realistic normal-light images. In addition to global and local adversarial losses, the global and local self feature preserving losses are proposed to preserve the image content before and after the enhancement. This is a key point for the stable training of such a one-path Generative Adversarial Network (GAN) structure.

**Zero-Shot Learning.** The supervised learning, reinforcement learning, and unsupervised learning methods either have limited generalization capability or suffer from unstable training. To remedy these issues, zero-shot learning is proposed to learn the enhancement solely from the testing images. Note that the concept of zero-shot learning in the low-level vision tasks is used to emphasize that the method does not require paired or unpaired training data, which is different from its definition in high-level visual tasks. Zhang et al. [24] propose a zero-shot learning method, called ExCNet, for back-lit image restoration. A network is first used to estimate the S-curve that best fits the input back-light image. Once the S-curve is estimated, the input image is separated into a base layer and a detail layer using the guided filter [57]. Then the base layer is adjusted by the estimated S-curve. Finally, the Weber contrast [58] is used to fuse the detailed layer and the adjusted base layer. To train the ExCNet, the authors formulate the loss function as a block-based energy minimization problem. Zhu et al. [26] propose a three-branch CNN, called RRDNet, for underexposed images restoration. The RRDNet decomposes an input image into illumination, reflectance, and noise via iteratively minimizing specially designed loss functions. To drive the zero-shot learning, a combination of retinex reconstruction loss, texture enhancement loss, and illumination-

guided noise estimation loss is proposed. Different from the image reconstruction-based methods [1], [3], [4], [11], [12], [21], [54], a deep curve estimation network, Zero-DCE, is proposed in [25]. Zero-DCE formulates the light enhancement as a task of image-specific curve estimation, which takes a low-light image as input and produces high-order curves as its output. These curves are used for pixel-wise adjustment on the dynamic range of the input to obtain an enhanced image. Further, an accelerated and light version is proposed, called Zero-DCE++ [59]. Such curve-based methods do not require any paired or unpaired data during training. They achieve zero-reference learning via a set of non-reference loss functions. Besides, unlike the image reconstruction-based methods that need high computational resources, the image-to-curve mapping only requires lightweight networks, thus achieving a fast inference speed.

**Semi-Supervised Learning.** To combine the strengths of supervised learning and unsupervised learning, semi-supervised learning has been proposed in recent years. Yang et al. [27] propose a semi-supervised deep recursive band network (DRBN). The DRBN first recovers a linear band representation of an enhanced image under supervised learning, and then obtains an improved one by recomposing the given bands via a learnable linear transformation based on unsupervised adversarial learning.

Observing Figure 3(a), we can find that supervised learning is the mainstream in the deep learning-based LLIE methods. The percentage reaches 77%. This is because supervised learning is relatively easy when paired training data such as LOL [4], SID [2] and diverse low-/normal-light image synthesis approaches are publicly available. However, supervised learning-based methods suffer from some challenges: **1)** collecting a large-scale paired dataset that covers diverse real-world low-light conditions is difficult, **2)** synthetic low-light images do not accurately represent real-world illuminance conditions such as spatially varying lighting and different levels of noise, and **3)** training a deep model on paired data may result in overfitting and limited generalization to real-world images of diverse illumination properties.

Therefore, some methods adopt unsupervised learning, reinforcement learning, semi-supervised learning, and zero-shot learning to bypass the challenges in supervised learning. Although these methods achieve competing performance, they still suffer from some limitations: **1)** for unsupervised learning/semi-supervised learning methods, how to implement stable training, avoid color deviations, and build the relations of cross-domain information challenges current methods, **2)** for reinforcement learning methods, designing an effective reward mechanism and implementing efficient and stable training are intricate, and **3)** for zero-shot learning methods, the design of non-reference losses is non-trivial when the color preservation, artifact removal, and gradient back-propagation should be taken into account.

### 3 TECHNICAL REVIEW AND DISCUSSION

In this section, we first summarize the representative deep learning-based LLIE methods in Table 1, then analyze and discuss their technical characteristics.

TABLE 1: Summary of essential characteristics of representative deep learning-based methods, including learning strategies, network structures, loss functions, training datasets, testing datasets, evaluation metrics, data formats of input, and whether the models are Retinex-based or not. “simulated” means the testing data are simulated by the same approach as the synthetic training data. “self-selected” stands for the real-world images selected by the authors. “#P” represents the number of trainable parameters. “-” means this item is not available or not indicated in the paper.

	Method	Learning	Network Structure	Loss Function	Training Data	Testing Data	Evaluation Metric	Format	Platform	Retinex
2017	LLNet [1]	SL	SSDA	SRR loss	simulated by Gamma Correction & Gaussian Noise	simulated self-selected	PSNR SSIM	RGB	Theano	
2018	LightenNet [5]	SL	four layers	$L_2$ loss	simulated by random illumination values	simulated self-selected	PSNR MAE SSIM User Study	RGB	Caffe MATLAB	✓
	Retinex-Net [4]	SL	multi-scale network	$L_1$ loss invariable reflectance loss smoothness loss SSIM loss	simulated by adjusting histogram	self-selected	-	RGB	TensorFlow	✓
	MBLLEN [3]	SL	multi-branch fusion	perceptual loss region loss	simulated by Gamma Correction & Poisson Noise	simulated self-selected	PSNR SSIM AB VIF LOE TOMI	RGB	TensorFlow	
	SCIE [6]	SL	frequency decomposition	$L_2$ loss $L_1$ loss SSIM loss	SCIE	SCIE	PSNR FSIM Runtime FLOPs	RGB	Caffe MATLAB	
	Chen et al. [2]	SL	U-Net	$L_1$ loss	SID	SID	PSNR SSIM	Raw	TensorFlow	
	Deepexposure [22]	RL	policy network GAN	deterministic policy gradient adversarial loss	MIT-Adobe FiveK	MIT-Adobe FiveK	PSNR SSIM	Raw	TensorFlow	
2019	Chen et al. [8]	SL	siamese network	$L_1$ loss self-consistency loss	DRV	DRV	PSNR SSIM MAE	Raw	TensorFlow	
	Jiang and Zheng [9]	SL	3D U-Net	$L_1$ loss	SMOID	SMOID	PSNR SSIM MSE	Raw	TensorFlow	
	DeepUPE [53]	SL	illumination map	$L_1$ loss smoothness loss color loss reflectance similarity loss illumination smoothness loss mutual consistency loss	retouched image pairs	MIT-Adobe FiveK	PSNR SSIM User Study	RGB	TensorFlow	✓
	KinD [11]	SL	three subnetworks U-Net	$L_1$ loss $L_2$ loss SSIM loss texture similarity loss illumination adjustment loss	LOL	LOL LIME NPE MEF	PSNR SSIM LOE NIQE	RGB	TensorFlow	✓
	Wang et al. [10]	SL	two subnetworks pointwise Conv U-Net like network	$L_1$ loss $L_2$ loss	simulated by camera imaging model MIT-Adobe FiveK	IP100 FNF38 MPI LOL NPE	PSNR SSIM NIQE	RGB	Caffe	✓
	Ren et al. [12]	SL	RNN dilated Conv	perceptual loss adversarial loss	simulated self-selected & Gaussian noise	DPED NPE LIME MEF DICM	PSNR SSIM Runtime	RGB	Caffe	
	EnlightenGAN [23]	UL	U-Net like network	adversarial loss self feature preserving loss	unpaired real images	VV BBD-100K ExDARK	User Study NIQE Classification	RGB	PyTorch	
	ExCNet. [24]	ZSL	fully connected layers	energy minimization loss	real images	$IE_{ps}D$	User Study CDIQA LOD	RGB	PyTorch	
2020	Zero-DCE [25]	ZSL	U-Net like network	spatial consistency loss exposure control loss color constancy loss illumination smoothness loss	SICE	SICE NPE LIME MEF DICM VV DARK FACE	User Study PI PSNR SSIM MAE Runtime Face detection	RGB	PyTorch	
	DRBN [27]	SSL	recursive network	SSIM loss perceptual loss adversarial loss	LOL images selected by MOS	LOL	PSNR SSIM SSIM-GC	RGB	PyTorch	
	Lv et al. [15]	SL	U-Net like network	Huber loss SSIM loss perceptual loss illumination smoothness loss	simulated by a retouching module	LOL SICE DeepUPE	User Study PSNR SSIM VIF LOE NIQE #P Runtime Face detection	RGB	TensorFlow	✓
	Fan et al. [14]	SL	four subnetworks U-Net like network feature modulation	mutual smoothness loss reconstruction loss illumination smoothness loss cross entropy loss consistency loss SSIM loss gradient loss ratio learning loss $L_2$ loss perceptual loss	simulated by illumination adjustment, slight color distortion, and noise simulation	simulated self-selected	PSNR SSIM NIQE	RGB	-	✓
	Xu et al. [50]	SL	frequency decomposition U-Net like network	$L_1$ loss	SID in RGB	SID in RGB self-selected	PSNR SSIM	RGB	PyTorch	
	EEMEFN [16]	SL	U-Net like network edge detection network	weighted cross-entropy loss	SID	SID	PSNR SSIM	Raw	TensorFlow PaddlePaddle	
	DLN [19]	SL	residual learning interactive factor back projection network	SSIM loss total variation loss	simulated by illumination adjustment, slight color distortion, and noise simulation	simulated LOL	User Study PSNR SSIM NIQE	RGB	PyTorch	
	LPNet [18]	SL	pyramid network	$L_1$ loss perceptual loss luminance loss	LOL SID in RGB MIT-Adobe FiveK	LOL SID in RGB MIT-Adobe FiveK MEF NPE DICM VV	PSNR SSIM NIQE #P FLOPs Runtime PSNR SSIM	RGB	PyTorch	
	SIDGAN [17]	SL	U-Net	CycleGAN loss	SIDGAN	SIDGAN	TPSNR TSSIM ATWE	Raw	TensorFlow	
	RRDNet [26]	ZSL	three subnetworks	retinex reconstruction loss texture enhancement loss noise estimation loss	-	NPE LIME MEF DICM	NIQE CPCQI	RGB	PyTorch	✓
	TBEFN [20]	SL	three stages U-Net like network	SSIM loss perceptual loss smoothness loss	SCIE LOL	SCIE LOL DICM MEF NPE VV	PSNR SSIM NIQE Runtime #P FLOPs	RGB	TensorFlow	✓
	DSLRL [21]	SL	Laplacian pyramid U-Net like network	$L_2$ loss Laplacian loss color loss	MIT-Adobe FiveK	MIT-Adobe FiveK self-selected	PSNR SSIM NIQMC NIQE BTMQI CaHDC	RGB	PyTorch	



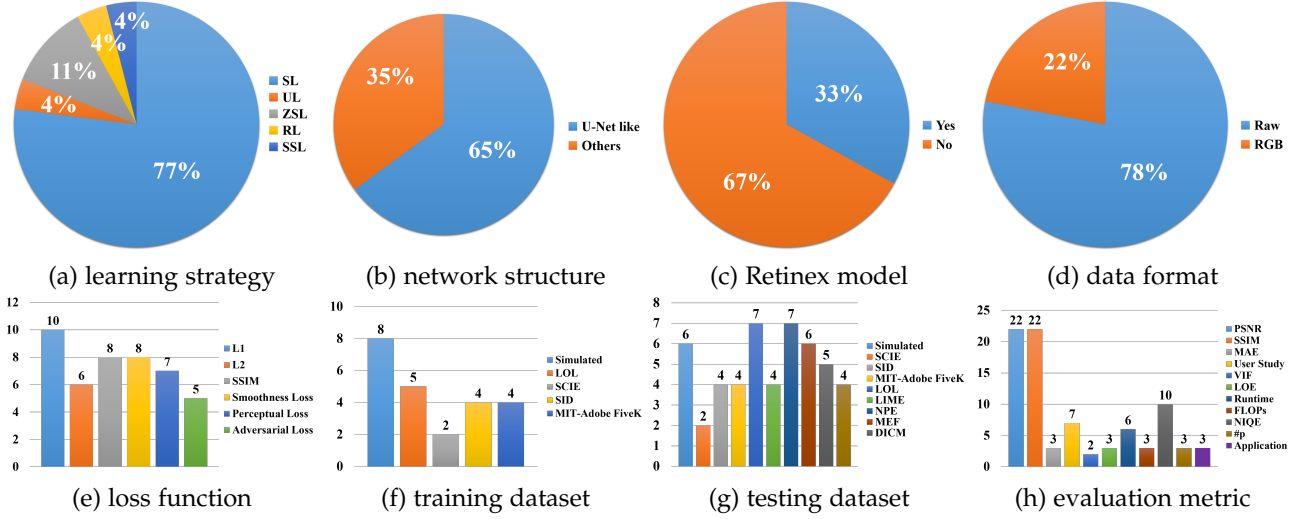


Fig. 3: A statistic analysis of deep learning-based LLIE methods, including learning strategy, network characteristic, Retinex model, data format, loss function, training dataset, testing dataset, and evaluation metric. Better to see with zoom.

### 3.1 Network Structure

Diverse network structures and designs have been used in the existing models, spanning from the basic U-Net, pyramid network, multi-stage network to frequency decomposition network. After analyzing Figure 3(b), it can be observed that the U-Net and U-Net-like networks are mainly adopted network structures in LLIE. This is because U-Net can effectively integrate multi-scale features and employ both low-level and high-level features. Such characteristics are essential for achieving satisfactory low-light enhancement.

Nevertheless, some key issues may be ignored in the current LLIE network structures: **1)** after going through several convolutional layers, the gradients of an extremely low light image may vanish during the gradient back-propagation due to its small pixel values. This would degrade the enhancement performance and affect the convergence of network training, **2)** the skip-connections used in the U-Net-like networks might introduce noise and redundant features into the final results. How to effectively filter out the noise and integrate both low-level and high-level features should be carefully considered, and **3)** although some designs and components are proposed for LLIE, most of them are borrowed or modified from related low-level visual tasks. The characteristics of low-light data should be considered when designing the network structures.

### 3.2 Combination of Deep Model and Retinex Theory

As presented in Figure 3(c), almost 1/3 of methods combine the designs of deep networks with the Retinex theory, e.g., designing different subnetworks to estimate the components of the Retinex model and estimating the illumination map to guide the learning of networks. Despite such a combination can bridge deep learning-based and model-based methods, their respective weaknesses may be introduced into the final models: **1)** the ideal assumption that the reflectance is the final enhanced result used in Retinex-based LLIE methods would still affect the final results, and **2)** the risk of overfitting in deep networks still exists in spite of

the introduction of Retinex theory. Therefore, how to cream off the best and filter out the impurities should be carefully considered when researchers combine deep learning with the Retinex theory.

### 3.3 Data Format

As shown in Figure 3(d), the Raw data format dominates most methods. Although Raw data are limited to specific sensors such as those based on Bayer patterns, the data cover wider color gamut and higher dynamic range. Hence, deep models trained on Raw data usually recover clear details and high contrast, obtain vivid color, reduce the effects of noises and artifacts, and improve the brightness of extremely low-light images. Nevertheless, the RGB format is also used in some methods because it is commonly found as the final imagery form produced by smartphone cameras, Go-Pro cameras, and drone cameras. In future research, a smooth transformation from the Raw data of different patterns to the RGB format would have the potentials to combine the convenience of RGB data and the advantage of high-quality enhancement of Raw data for LLIE.

### 3.4 Loss Function

In Figure 3(e), the commonly adopted loss functions in LLIE models include reconstruction loss ( $L_1$ ,  $L_2$ , SSIM), perceptual loss, and smoothness loss. Besides, according to different demands and formulations, the color loss, exposure loss, and adversarial loss are also adopted. We detail representative loss functions as follows.

**Reconstruction Loss.** The commonly used  $L_1$ ,  $L_2$ , and SSIM losses can be expressed as:

$$L_1 = \frac{1}{HWC} \sum_{i=1}^H \sum_{j=1}^W \sum_{c=1}^C \|R(i, j) - \hat{R}(i, j)\|_1, \quad (3)$$

$$L_2 = \frac{1}{HWC} \sum_{i=1}^H \sum_{j=1}^W \sum_{c=1}^C \|R(i, j) - \hat{R}(i, j)\|_2^2, \quad (4)$$

$$L_{ssim} = 1 - \frac{(2\mu_R\mu_{\hat{R}} + c_1)(2\sigma_{R\hat{R}} + c_2)}{(\mu_R^2 + \mu_{\hat{R}}^2 + c_1)(\sigma_R^2 + \sigma_{\hat{R}}^2 + c_2)}, \quad (5)$$

where  $R$  and  $\hat{R}$  respectively represent the ground truth and the enhanced result,  $H$ ,  $W$ , and  $C$  are the height, width, and channel of input image, respectively. Mean and variance are represented by  $\mu$  and  $\sigma$ , respectively. The constant  $c_1$  and  $c_2$  are set to 0.02 and 0.03 based on the default values in the SSIM loss [60]. Different reconstruction losses have their advantages and disadvantages.  $L_2$  loss tends to penalize larger errors, but is tolerant to small errors.  $L_1$  loss preserves colors and luminance well since an error is weighed equally regardless of the local structure.  $L_{ssim}$  loss preserves the structure and texture well. Refer to [61] for detailed analysis.

**Perceptual Loss.** Perceptual loss [62] is proposed to constrain the results similar with the ground truth in the feature space. The loss improves the visual quality of results. It is defined as the Euclidean distance between the feature representations of an enhanced result and those of corresponding ground truth. The feature representations are typically extracted from the VGG network [63] pre-trained on ImageNet dataset [64]. The perceptual loss  $L_{per}$  can be expressed as:

$$L_{per} = \frac{1}{PQN} \sum_{i=1}^P \sum_{j=1}^Q \sum_{n=1}^N \|\phi_j(R)(i, j) - \phi_j(\hat{R})(i, j)\|^2, \quad (6)$$

where  $P$ ,  $Q$ , and  $N$  are the height, width, and channel number of feature maps, respectively. The function  $\phi_j$  represents the feature representations extracted from the  $j$ th convolutional layer (after ReLU activation) of VGG network.

**Smoothness Loss.** To remove noise in the enhanced results or preserve the relationship of neighboring pixels, smoothness loss (TV loss)  $L_{tv}$  is often used to constrain the enhanced result or the estimated illumination map, which can be expressed as:

$$L_{tv} = \frac{1}{HWC} \sum_{i=1}^H \sum_{j=1}^W \sum_{c=1}^C (\|\Delta_x \hat{R}\| + \|\Delta_y \hat{R}\|), \quad (7)$$

where  $\Delta_x$  and  $\Delta_y$  are the horizontal and vertical gradient operations, respectively.

**Adversarial Loss.** To encourage enhanced results to be indistinguishable from reference images, adversarial learning solves the following optimization problem:

$$\min_G \max_{D_g} \mathbb{E}_{I \sim S} [\log(1 - D(G(I)))] + \mathbb{E}_{R \sim T} [\log(D(R))], \quad (8)$$

where the generator  $G$  tries to generate ‘fake’ images to fool the discriminator  $D$ . The discriminator  $D$  tries to distinguish ‘fake’ images from the reference images. The input  $I$  is sampled from the source manifold  $S$  while  $R$  is an arbitrary reference image sampled from the target manifold  $T$ . To optimize the generator, this loss function should be minimized:

$$L_G = \log(1 - D(G(I))), \quad (9)$$

where  $G(I)$  outputs an enhanced result. To optimize the discriminator, this loss function is minimized:

$$L_D = -\log(1 - D(G(I))) - \log(D(R)). \quad (10)$$

**Exposure Loss.** As one of key loss functions in ZSL-based LLIE methods, the exposure loss  $L_{exp}$  measures the exposure levels of enhanced results without paired or unpaired images as reference images, which can be expressed as:

$$L_{exp} = \frac{1}{M} \sum_{k=1}^M \|Y_k - E\|, \quad (11)$$

where  $M$  is the number of non-overlapping regions of a fixed size ( $16 \times 16$  by default) and  $Y$  is the average intensity value of a region in the enhanced result.

The commonly used loss functions in LLIE networks, such as  $L_1$ ,  $L_2$ , SSIM, perceptual losses, are also employed in image reconstruction networks for image super-resolution [65], image denoising [66], image detraining [67], [68], and image deblurring [69]. Different from these versatile losses, the specially designed exposure loss for LLIE inspires the design of non-reference losses. A non-reference loss does not rely on reference images, thus making a model enjoying better generalization capability. It is an on-going research to take image characteristics into account for the design of loss functions.

### 3.5 Training Datasets

Figure 3(f) reports the usage of a variety of paired training datasets for training low-light enhancement networks. These datasets include real-world captured datasets and synthetic datasets. We list them in Table 2 and introduce them in detail as follows.

**Simulated by Gamma Correction.** Owing to its nonlinearity and simplicity, Gamma correction is used to adjust the luminance or tristimulus values in video or still image systems. It is defined by a power-law expression:

$$V_{out} = AV_{in}^\gamma, \quad (12)$$

where the input  $V_{in}$  and output  $V_{out}$  are typically in the range of  $[0, 1]$ . The constant  $A$  is set to 1 in the common case. The power  $\gamma$  controls the luminance of the output. Intuitively, the input is brightened when  $\gamma < 1$  while the input is darkened when  $\gamma > 1$ . The input can be the three RGB channels of an image or the luminance-related channels such as  $L$  channel in the CIE Lab color space and  $Y$  channel in the YCbCr color space. After adjusting the luminance-related channel using Gamma correction, the corresponding channels in the color space are adjusted by equal proportion to avoid producing artifacts and color deviations.

To simulate images taken in real-world low-light scenes, Gaussian noise, Poisson noise, or realistic noise is added to the Gamma corrected images. The low-light image synthesized using Gamma correction can be expressed as:

$$I_{low} = n(g(I_{in}; \gamma)), \quad (13)$$

where  $n$  represents the noise model,  $g(I_{in}; \gamma)$  represents the Gamma correction function with Gamma value  $\gamma$ ,  $I_{in}$  is a normal-light and high-quality image or luminance-related channel. Although this function produces low-light images of different lighting levels by changing the Gamma value  $\gamma$ , it tends to introduce artifacts and color deviations into the synthetic low-light images due to the nonlinear adjustment.

TABLE 2: Summary of paired training datasets. ‘Syn’ represents Synthetic.

Name	Number	Format	Real/Syn	Video
Gamma Correction	$+\infty$	RGB	Syn	
Random Illumination	$+\infty$	RGB	Syn	
LOL [4]	500	RGB	Real	
SCIE [6]	4,413	RGB	Real	
VE-LOL-L [48]	2,500	RGB	Real+Syn	
MIT-Adobe FiveK [70]	5,000	Raw	Real	
SID [4]	5,094	Raw	Real	
DRV [8]	202	Raw	Real	✓
SMOID [9]	179	Raw	Real	✓

**Simulated by Random Illumination.** According to the Retinex model, an image can be decomposed into a reflectance component and an illumination component. Based on the assumption that image content is independent of illumination component and local region in the illumination component have the same intensity, a low-light image can be obtained by

$$I_{low} = I_{in}L, \quad (14)$$

where  $L$  is a random illumination value in the range of  $[0,1]$ . Noises can be added to the synthetic images. Such a linear function avoids artifacts, but the strong assumption requires the synthesis to operate only on image patches where local regions have the same brightness. A deep model trained on such image patches may lead to sub-optimal performance due to the negligence of context information.

**LOL.** LOL [4] is the first paired low-/normal-light image dataset taken in real scenes. The low-light images are collected by changing the exposure time and ISO. LOL contains 500 pairs of low-/normal-light images of size  $400 \times 600$  saved in RGB format.

**SCIE.** SCIE is a multi-exposure image dataset of low-contrast and good-contrast image pairs. It includes multi-exposure sequences of 589 indoor and outdoor scenes. Each sequence has 3 to 18 low-contrast images of different exposure levels, thus containing 4,413 multi-exposure images in total. The 589 high-quality reference images are obtained by selecting from the results of 13 representative enhancement algorithms. That is many multi-exposure images have the same high-contrast reference image. The image resolutions are between  $3,000 \times 2,000$  and  $6,000 \times 4,000$ . The images in SCIE are saved in RGB format.

**MIT-Adobe FiveK.** MIT-Adobe FiveK [70] was collected for global tone adjustment but has been used in LLIE. This is because the input images have low light and low contrast. MIT-Adobe FiveK contains 5,000 images, each of which is retouched by 5 trained photographers towards visually pleasing renditions, akin to a postcard. Thus, each input has five retouched results. Typically, the results of expert C are used as the ground truth images during the training phase. The images are all in Raw format. To train the networks that can handle images of RGB format, one needs to use Adobe Lightroom to pre-process the images and save them as RGB format following this procedure<sup>1</sup>. The images are commonly resized to have a long-edge of 500 pixels.

**SID.** SID [2] contains 5,094 Raw short-exposure images, each with a corresponding long-exposure reference image. The number of distinct long-exposure reference images is

424. In other words, multiple short-exposure images correspond to the same long-exposure reference image. The images were taken using two cameras: Sony  $\alpha 7S$  II and Fujifilm X-T2 in both indoor and outdoor scenes. Thus, the images have different sensor patterns (Sony camera’s Bayer sensor and Fuji camera’s APS-C X-Trans sensor). The resolution is  $4,240 \times 2,832$  for Sony and  $6,000 \times 4,000$  for Fuji. Usually, the long-exposure images are processed by libraw (a raw image processing library) and saved in the sRGB color space, and randomly cropped  $512 \times 512$  patches for training.

**VE-LOL.** VE-LOL [48] consists two subsets: paired VE-LOL-L that is used for training and evaluating LLIE methods and unpaired VE-LOL-H that is used for evaluating the effect of LLIE methods on face detection. Specifically, VE-LOL-L includes 2,500 paired images. Among them, 1,000 pairs are synthetic, while 1,500 pairs are real. VE-LOL-H includes 10,940 unpaired images, where human faces are manually annotated with bounding boxes.

**DRV.** DRV [8] contains 202 static raw videos, each of which has a corresponding long-exposure ground truth. Each video was taken at approximately 16 to 18 frames per second in a continuous shooting mode and is with up to 110 frames. The images were taken by a Sony RX100 VI camera in both indoor and outdoor scenes, thus all in the Bayer Raw format. The resolution is  $3,672 \times 5,496$ .

**SMOID.** SMOID [9] contains 179 pairs of videos taken by a co-axis optical system, each of which has 200 frames. Thus, SMOID includes 35,800 extremely low light Bayer Raw images and their corresponding well-lightened RGB counterparts. The videos in SMOID consist of moving vehicles and pedestrians under different illumination conditions.

Some issues challenge the aforementioned paired training datasets: **1)** deep models trained on synthetic data may introduce artifacts and color deviations when processing real-world images and videos due to the gap between synthetic data and real data, **2)** the scale and diversity of real training data are unsatisfactory, thus some methods incorporate synthetic data to augment the training data. This may lead to sub-optimal enhancement, and **3)** the input images and corresponding ground truths may exist misalignment due to the effects of motion, hardware, and environment. This would affect the performance of deep networks trained using pixel-wise loss functions.

### 3.6 Testing Datasets

In addition to the testing subsets in the paired datasets [2], [4], [6], [8], [9], [48], [70], there are several testing data collected from related works or commonly used for experimental comparisons. They are collected from LIME [32], NPE [30], MEF [71], DICM [72], and VV<sup>2</sup>. Besides, some datasets such as face detection in the dark [73] and detection and recognition in low-light images [74] are employed to test the effects of LLIE on high-level visual tasks. We summarize the commonly used testing datasets in Table 3 and introduce the representative testing datasets as follows.

**BBD-100K.** BBD-100K [75] is the largest driving video dataset with 10,000 videos taken over 1,100-hour driving experience across many different times in the day, weather

1. <https://github.com/sjmoran/DeepLPP>

2. <https://sites.google.com/site/vonikakis/datasets>



TABLE 3: Summary of testing datasets.

Name	Number	Format	Application	Video
LIME [32]	10	RGB		
NPE [30]	84	RGB		
MEF [71]	17	RGB		
DICM [72]	64	RGB		
VV	24	RGB		
BBD-100K [75]	10,000	RGB	✓	✓
ExDARK [74]	7,363	RGB	✓	
DARK FACE [73]	6,000	RGB	✓	
VE-LOL-H [48]	10,940	RGB	✓	

conditions, and driving scenarios, and 10 tasks annotations. The videos taken at nighttime in BBD-100K are used to validate the effects of LLIE on high-level visual tasks and the enhancement performance in real scenarios.

**ExDARK.** ExDARK [74] dataset is built for object detection and recognition in low-light images. ExDARK dataset contains 7,363 low-light images from extremely low-light environments to twilight with 12 object classes annotated with both image class label and local object bounding boxes.

**DARK FACE.** DARK FACE [73] dataset contains 6,000 low-light images captured in outdoor scenes during the nighttime, each of which is labeled with bounding boxes of human face.

From Figure 3(g), we can observe that one prefers using the self-collected testing data in the experiments. The main reasons lie into three-fold: **1)** besides the test partition of paired datasets, there is no acknowledged benchmark for evaluations, **2)** the commonly used test sets suffer from some shortcomings such as small scale (some test sets contain 10 images only), repeated content and illumination properties, and unknown experimental settings, and **3)** some of commonly used testing data are not originally collected for evaluating LLIE. In general, current testing datasets may lead to bias and unfair comparisons.

### 3.7 Evaluation Metrics

Besides human perception-based subjective evaluations, image quality assessment (IQA) metrics, including both full-reference and non-reference IQA metrics, are able to evaluate image quality objectively. In addition, user study, number of trainable parameters, FLOPs, runtime, and application-based evaluations also reflect the performance of LLIE models, as shown in Fig. 3(h). We will detail them as follows.

**PSNR and MSE.** PSNR and MSE are widely used IQA metrics in low-level visual tasks. They are always non-negative, and values closer to infinite (PSNR) and zero (MSE) are better. Nevertheless, the pixel-wise PSNR and MSE may provide inaccurate indication of the visual perception of image quality since they neglect of the relation of neighbouring pixels.

**MAE.** MAE represents the mean absolute error, serving as a measure of errors between paired observations. The smaller the MAE value is, the better similarity is.

**SSIM.** SSIM is used to measure the similarity between two images. It is a perception-based model that considers image degradation as perceived change in structural information. The value 1 is only reachable in the case of two identical sets of data, indicating perfect structural similarity.

**LOE.** LOE represents the lightness order error that reflects the naturalness of an enhanced image. For LOE, the smaller the LOE value is, the better the lightness order is preserved. **Application.** Besides improving the visual quality, one of the purposes of image enhancement is to serve the high-level visual task. Thus, the effects of LLIE on high-level visual applications are commonly examined to validate the performance of different methods.

The current evaluation approaches used in LLIE need to be improved in several aspects: **1)** although the PSNR, MSE, MAE, and SSIM are classic and popular metrics, they are still far from capturing real visual perception of human, **2)** some metrics are not originally designed for low-light images. They are used for assessing the fidelity of image information and contrast. Using these metrics may reflect the image quality, but they are far from the real purpose of low-light enhancement, **3)** metrics specially designed for low-light images are lacking, except for the LOE metric. Moreover, there is no metric for evaluating low-light video enhancement, and **4)** a metric that can balance both the human vision and the machine perception is expected.

## 4 BENCHMARKING AND EMPIRICAL ANALYSIS

This section provides empirical analysis and highlight some key challenges in deep learning-based LLIE. To facilitate the analysis, we propose a large-scale low-light image and video dataset to examine the performance of different deep learning-based solutions. In addition, we develop the first online platform, where the results of deep learning-based LLIE models can be produced via a user-friendly web interface. In this section, we conduct extensive evaluations on several benchmarks and our proposed dataset.

In the experiments, we compare 13 representative methods, including seven supervised learning-based methods (LLNet [1], LightenNet [5], Retinex-Net [4], MBLLEN [3], KinD [11], KinD++ [54], TBEFN [20], DSLR [21]), one unsupervised learning-based method (EnlightenGAN [23]), one semi-supervised learning-based method (DRBN [27]), and three zero-shot learning-based methods (ExCNet [24], ZeroDCE [25], RRDNet [26]). We use the publicly available codes to produce their results for fair comparisons.

### 4.1 A New Low-Light Image and Video Dataset

We propose a large-scale low-light image and video dataset, called LoLi-Phone, to comprehensively and thoroughly validate the performance of LLIE methods. LoLi-Phone is the largest and most challenging real-world testing dataset of its kind. In particular, the dataset contains 120 videos (55,148 images) taken by 18 different mobile phones' cameras including iPhone 6s, iPhone 7, iPhone7 Plus, iPhone8 Plus, iPhone 11, iPhone 11 Pro, iPhone XS, iPhone XR, iPhone SE, Xiaomi Mi 9, Xiaomi Mi Mix 3, Pixel 3, Pixel 4, Oppo R17, Vivo Nex, LG M322, OnePlus 5T, Huawei Mate 20 Pro under diverse illumination conditions (e.g., weak lighting, underexposure, moonlight, twilight, dark, extremely dark, back-lit, non-uniform light, and colored light.) in both indoor and outdoor scenes. A summary of LoLi-Phone dataset is provided in Table 4. We present several samples of LoLi-Phone dataset in Figure 4. We will release the proposed LoLi-Phone dataset.

TABLE 4: Summary of LoLi-Phone dataset. LoLi-Phone dataset contains 120 videos (55,148 images) taken by 18 different mobile phones’ cameras. “#Video” and “#Image” represent the number of videos and images, respectively.

Phone’s Brand	#Video	#Image	Resolution
iPhone 6s	4	1,029	1920×1080
iPhone 7	13	6,081	1920×1080
iPhone7 Plus	2	900	1920×1080
iPhone8 Plus	1	489	1280×720
iPhone 11	7	2,200	1920×1080
iPhone 11 Pro	17	7,739	1920×1080
iPhone XS	11	2,470	1920×1080
iPhone XR	16	4,997	1920×1080
iPhone SE	1	455	1920×1080
Xiaomi Mi 9	2	1,145	1920×1080
Xiaomi Mi Mix 3	6	2,972	1920×1080
Pixel 3	4	1,311	1920×1080
Pixel 4	3	1,1923	1920×1080
Oppo R17	6	2,126	1920×1080
Vivo Nex	12	4,097	1280×720
LG M322	2	761	1920×1080
OnePlus 5T	1	293	1920×1080
Huawei Mate 20 Pro	12	4,160	1920×1080

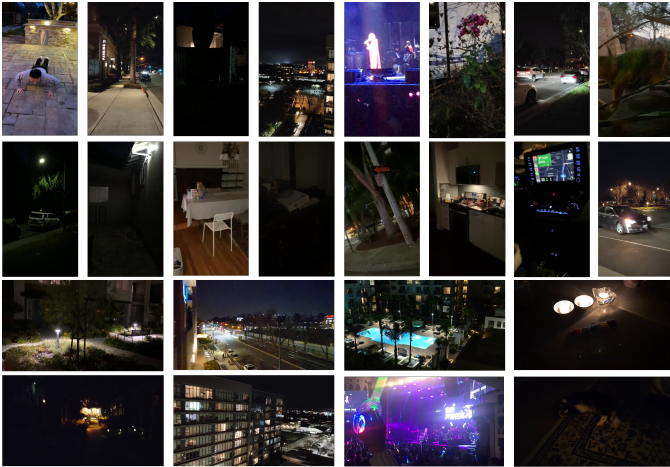


Fig. 4: Several images sampled from the proposed LoLi-Phone dataset. The images and videos are taken by different devices under diverse lighting conditions and scenes.

This challenging dataset is collected in real scenes and contains diverse low-light images and videos. Consequently, it is suitable for evaluating the generalization capability of different low-light image and video enhancement models. Notably, the dataset can be used as the training dataset for unsupervised learning-based methods and the reference dataset for synthesis methods to generate realistic low-light images and videos.

## 4.2 Online Evaluation Platform

Different deep models may be implemented in different deep learning platforms such as Caffe, Theano, TensorFlow, and PyTorch. As a results, different algorithms demand for different configurations, GPU versions and hardware specifications. Such requirements are prohibitive to many researchers, especially for beginners who are new to this area and may not even have GPU resources. To resolve these problems, we develop a LLIE online platform, called LoLi-Platform. The platform is available at <http://mc.nankai.edu.cn/ll/>.

To the date of this submission, the LoLi-Platform covers 13 popular deep learning-based LLIE methods including LLNet [1], LightenNet [5], Retinex-Net [4], EnlightenGAN [23], MBLEN [3], KinD [11], KinD++ [54], TBEFN [20], DSLR [21], DRBN [27], ExCNet [24], Zero-DCE [25], and RRDNet [26], where the results of any input can be produced through a user-friendly web interface. We will regularly offer new methods on this platform. We wish that this LoLi-Platform could serve the growing research community by providing users a flexible interface to run existing deep learning-based LLIE methods and develop their own new LLIE methods.

## 4.3 Benchmarking Results

To qualitatively and quantitatively evaluate different methods, in addition to the proposed LoLi-Phone dataset, we also adopt the commonly used LOL [4] and MIT-Adobe FiveK [70] datasets. More visual results can be found in the supplementary material. Moreover, the comparison results on the real low-light videos taken by different mobile phones’ cameras can be found at YouTube <https://www.youtube.com/watch?v=Elo9TKrG5Oo&t=6s>.

Specifically, we select five images in average from each video of LoLi-Phone dataset, forming an image testing dataset with a total of 600 images (denoted as LoLi-Phone-imgT). Furthermore, we randomly select one video from the videos of each phone’s brand of LoLi-Phone dataset, forming a video testing dataset with a total of 18 videos (denoted as LoLi-Phone-vidT). We half the resolutions of the frames in both LoLi-Phone-imgT and LoLi-Phone-vidT because some deep learning-based methods cannot process the full resolution of test images and videos. For the LOL dataset, we adopt the original test set including 15 low-light images captured in real scenes for testing, denoted as LOL-test. For the MIT-Adobe FiveK dataset, we follow the processing in [40] to decode the images into the PNG format and resize them to have a long-edge of 512 pixels using Lightroom. We adopt the same testing dataset as [40], MIT-Adobe FiveK-test, including 500 images with the retouching results by experts C as the corresponding ground truths.

**Qualitative Comparison.** We first present the results of different methods on the images sampled from LOL-test and MIT-Adobe FiveK-test datasets in Figures 5 and 6.

As shown in Figure 5, all methods improve the brightness and contrast of the input image. However, none of them successfully recovers the accurate color of the input image when the results are compared with the ground truth. In particular, LLNet [1] produces blurring result. LightenNet [5] and RRDNet [26] produce under-exposed results while MBLEN [3] and ExCNet [24] tend to over-expose the image. KinD [11], KinD++ [54], TBEFN [20], DSLR [21], EnlightenGAN [23], and DRBN [27] introduce obvious artifacts.

In Figure 6, LLNet [5], KinD++ [54], TBEFN [20], and RRDNet [26] produce over-exposed results. Retinex-Net [4], KinD++ [54], and RRDNet [26] yield artifacts and blurring in the results. We found that the ground truths of MIT-Adobe FiveK dataset still contain some dark regions. This is because the dataset is originally designed for global image retouching, where restoring low light regions is not the main priority in this task.



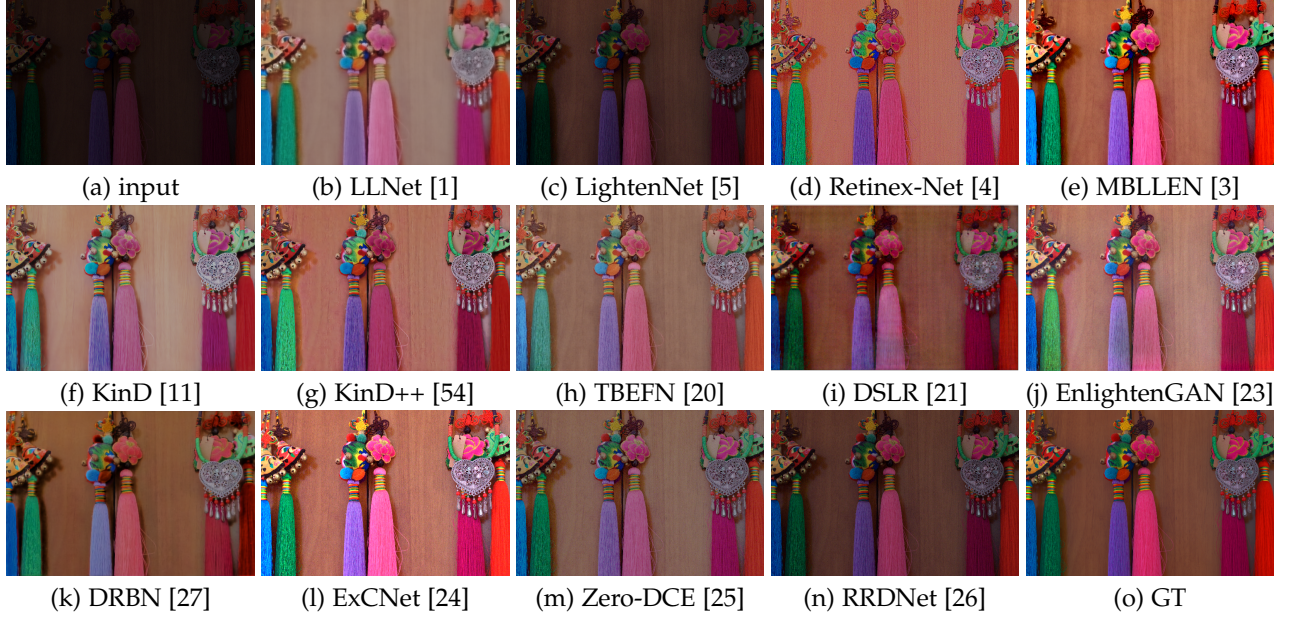


Fig. 5: Visual results of different methods on a low-light image sampled from LOL-test dataset.

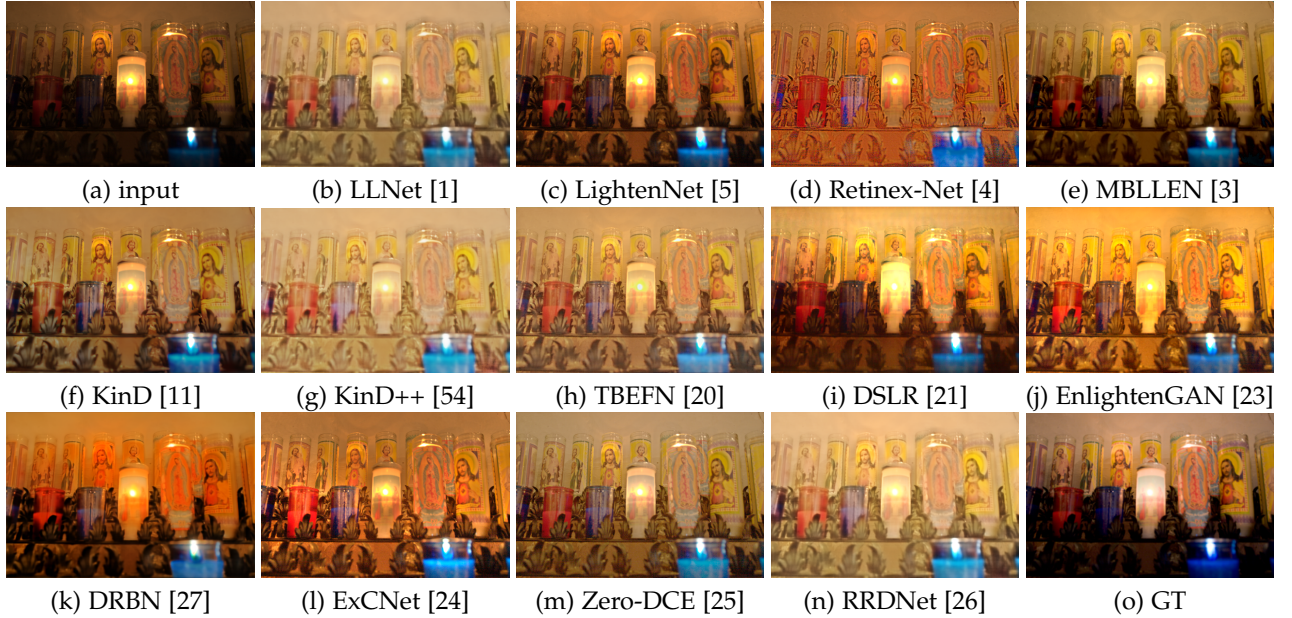


Fig. 6: Visual results of different methods on a low-light image sampled from MIT-Adobe FiveK-test dataset.

We also observed that the input images in LOL dataset and MIT-Adobe FiveK dataset are relatively clean from noise, which is different from real low-light scenes. Although some LLIE methods [18], [21], [53] take the MIT-Adobe FiveK dataset as training or testing dataset, we argue that this dataset is not appropriate for the task of LLIE due to its mis-matched/unsatisfactory ground truth for LLIE.

To examine the generalization capability of different methods, we conduct comparisons on the images sampled from our LoLi-Phone-imgT dataset. The visual results of different methods are shown in Figures 7 and 8. As presented in Figure 7, all methods cannot effectively improve the brightness and remove the noise of the input low-light

image. Moreover, Retinex-Net [4], MBLLEN [3], and DRBN [27] produce obvious artifacts. In Figure 8, all methods enhance the brightness of this input image. However, only MBLLEN [3] and RRDNet [26] obtain visually pleasing enhancement without color deviation, artifacts, and over-/under-exposure. Notably, for regions with the light source, none of the methods can brighten the image without amplifying the noise around these regions. Taking light sources into account for LLIE would be an interesting direction to explore. The results suggest the difficulty of enhancing the images of the LoLi-Phone-imgT dataset.

**Quantitative Comparison.** For testing sets with ground truth i.e., LOL-test and MIT-Adobe FiveK-test, we adopt



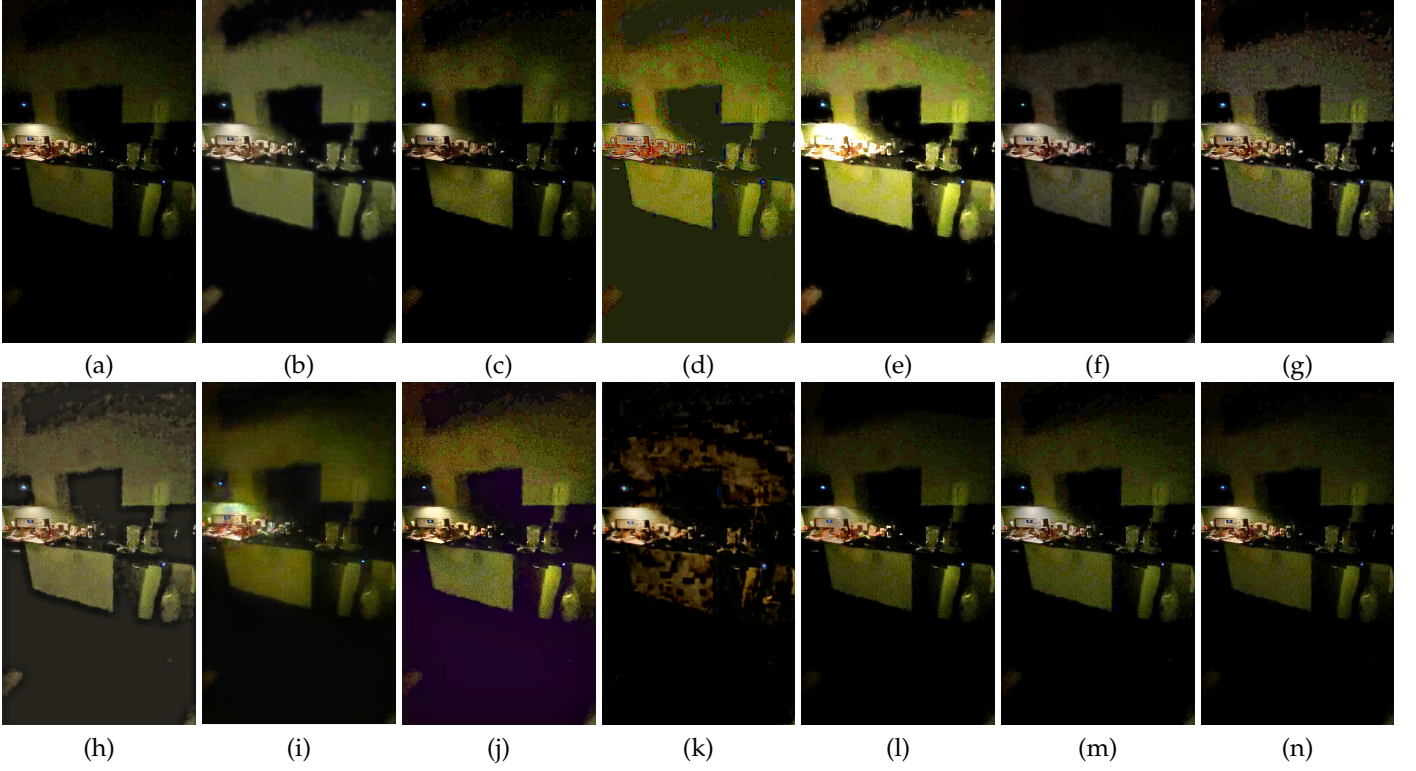


Fig. 7: Visual results of different methods on a low-light image sampled from LoLi-Phone-imgT dataset. (a) input. (b) LLNet [1]. (c) LightenNet [5]. (d) Retinex-Net [4]. (e) MBLLEN [3]. (f) KinD [11]. (g) KinD++ [54]. (h) TBEFN [20]. (i) DSLR [21]. (j) EnlightenGAN [23]. (k) DRBN [27]. (l) ExCNet [24]. (m) Zero-DCE [25]. (n) RRDNet [26].

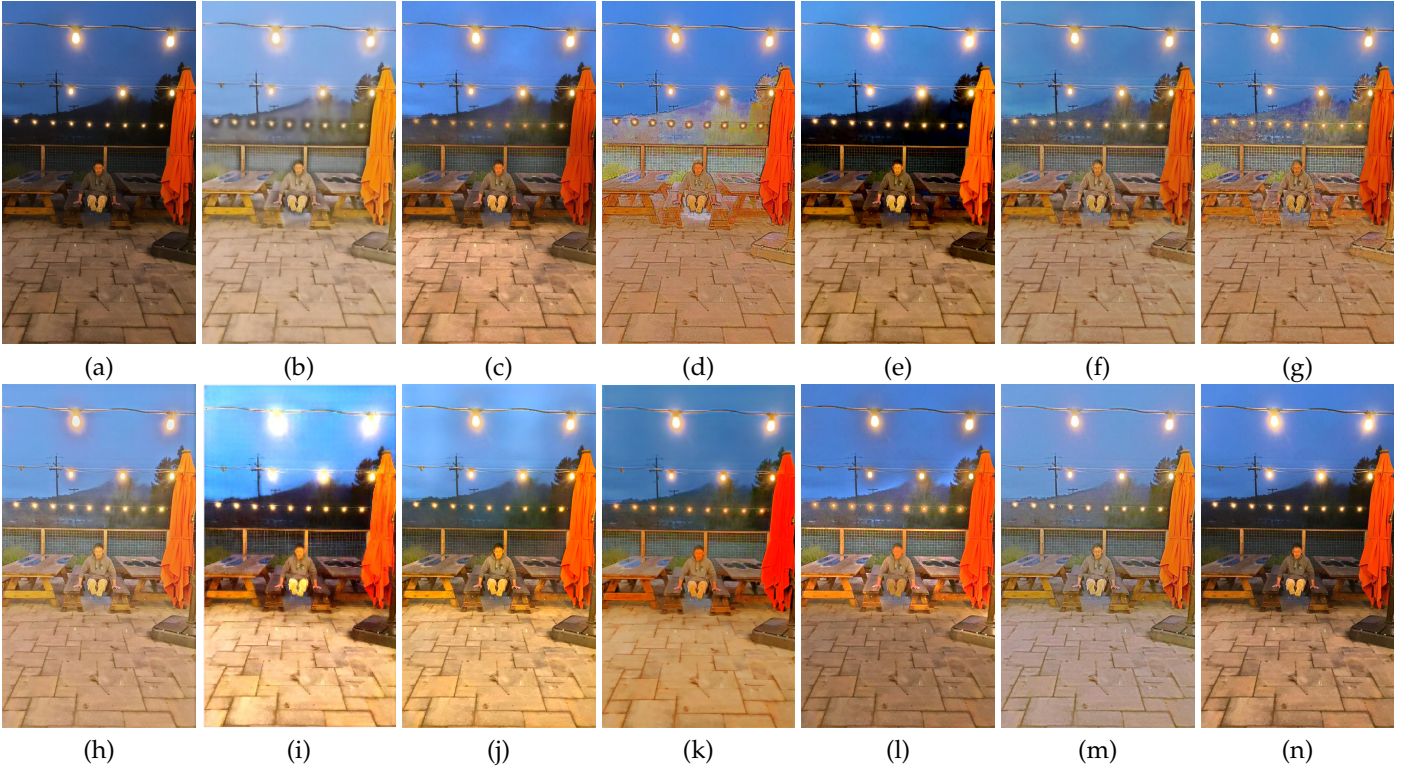


Fig. 8: Visual results of different methods on a low-light image sampled from LoLi-Phone-imgT dataset. (a) input. (b) LLNet [1]. (c) LightenNet [5]. (d) Retinex-Net [4]. (e) MBLLEN [3]. (f) KinD [11]. (g) KinD++ [54]. (h) TBEFN [20]. (i) DSLR [21]. (j) EnlightenGAN [23]. (k) DRBN [27]. (l) ExCNet [24]. (m) Zero-DCE [25]. (n) RRDNet [26].

TABLE 5: Quantitative comparisons on LOL-test and MIT-Adobe FiveK-test testing datasets in terms of MSE ( $\times 10^3$ ), PSNR (in dB), SSIM [60], and LPIPS [76]. The best result is in **red** whereas the second and third best results are in **blue** and **purple** under each case, respectively.

Learning	Method	LOL-test				MIT-Adobe FiveK-test			
		MSE↓	PSNR↑	SSIM↑	LPIPS↓	MSE↓	PSNR↑	SSIM↑	LPIPS↓
	input	12.613	7.773	0.181	0.560	<b>1.670</b>	<b>17.824</b>	<b>0.779</b>	<b>0.148</b>
SL	LLNet [1]	<b>1.290</b>	<b>17.959</b>	0.713	0.360	4.465	12.177	0.645	0.292
	LightenNet [5]	7.614	10.301	0.402	0.394	4.127	13.579	0.744	<b>0.166</b>
	Retinex-Net [4]	1.651	16.774	0.462	0.474	4.406	12.310	0.671	0.239
	MBLLEN [3]	1.444	<b>17.902</b>	0.715	0.247	<b>1.296</b>	<b>19.781</b>	<b>0.825</b>	<b>0.108</b>
	KinD [11]	<b>1.431</b>	17.648	<b>0.779</b>	<b>0.175</b>	2.675	14.535	0.741	0.177
	KinD++ [54]	<b>1.298</b>	<b>17.752</b>	<b>0.760</b>	<b>0.198</b>	7.582	9.732	0.568	0.336
	TBEFN [20]	1.764	17.351	<b>0.786</b>	<b>0.210</b>	3.865	12.769	0.704	0.178
	DSLRL [21]	3.536	15.050	0.597	0.337	<b>1.925</b>	<b>16.632</b>	<b>0.782</b>	0.167
UL	EnlightenGAN [23]	1.998	17.483	0.677	0.322	3.628	13.260	0.745	0.170
SSL	DRBN [27]	2.359	15.125	0.472	0.316	3.314	13.355	0.378	0.281
ZSL	ExCNet [24]	2.292	15.783	0.515	0.373	2.927	13.978	0.710	0.187
	Zero-DCE [25]	3.282	14.861	0.589	0.335	3.476	13.199	0.709	0.203
	RRDNet [26]	6.313	11.392	0.468	0.361	7.057	10.135	0.620	0.303

MSE, PSNR, SSIM [60], and LPIPS [76] metrics to quantitatively compare different methods. LPIPS [76] is a deep learning-based image quality assessment metric that measures the perceptual similarity between a result and its corresponding ground truth by deep visual representations. For LPIPS, we employ the AlexNet-based model to compute the perceptual similarity. A lower LPIPS value suggests a result that is closer to the corresponding ground truth in terms of perceptual similarity. In Table 5, we show the quantitative results.

As presented in Table 5, the quantitative scores of supervised learning-based methods are better than those of unsupervised learning-based, semi-supervised learning-based, and zero-shot learning-based methods on LOL-test and MIT-Adobe FiveK-test datasets. Among them, LLNet [1] obtains the best MSE and PSNR values on LOL-test dataset; however, its performance drops on MIT-Adobe FiveK-test dataset. This may be caused the bias of LLNet [1] towards the LOL dataset since it was trained using LOL training dataset. For LOL-test dataset, TBEFN [20] obtains the highest SSIM value while KinD [11] achieves the lowest LPIPS value. There is no winner across these four evaluation metrics on LOL-test dataset despite the fact that some methods were trained on LOL training dataset. For MIT-Adobe FiveK-test dataset, MBLLEN [3] outperforms all compared methods under the four evaluation metrics in spite of being trained on synthetic training data. Nevertheless, MBLLEN [3] still cannot obtain the best performance on both two testing datasets.

For LoLi-Phone-imgT testing set, we use the non-reference image quality assessment metrics, i.e., NIQE [77], perceptual index (PI) [77], [78], [79], LOE [30], and SPAQ [80] to quantitatively compare different methods. In terms of LOE, the smaller the LOE value is, the better the lightness order is preserved. For NIQE, the smaller the NIQE value is, the better the visual quality is. A lower PI value indicates better perceptual quality. SPAQ is devised for the perceptual quality assessment of smartphone photography. A larger SPAQ value suggests better perceptual quality of a smartphone photography. The quantitative results are provided in Table 6.

Observing Table 6, we can find that the performance

TABLE 6: Quantitative comparisons on LoLi-Phone-imgT dataset in terms of NIQE [77], LOE [30], PI [77], [78], [79], and SPAQ [80]. The best result is in **red** whereas the second and third best results are in **blue** and **purple** under each case, respectively.

Learning	Method	LoLi-Phone-imgT			
		NIQE↓	LOE↓	PI↓	SPAQ↑
	input	6.99	<b>0.00</b>	5.86	44.45
SL	LLNet [1]	5.86	<b>5.86</b>	5.66	40.56
	LightenNet [5]	5.34	952.33	4.58	45.74
	Retinex-Net [4]	5.01	790.21	<b>3.48</b>	<b>50.95</b>
	MBLLEN [3]	5.08	220.63	4.27	42.50
	KinD [11]	4.97	405.88	4.37	44.79
	KinD++ [54]	<b>4.73</b>	681.97	<b>3.99</b>	<b>46.89</b>
	TBEFN [20]	4.81	552.91	4.30	44.14
	DSLRL [21]	<b>4.77</b>	447.98	4.31	41.08
UL	EnlightenGAN [23]	<b>4.79</b>	821.87	<b>4.19</b>	45.48
SSL	DRBN [27]	5.80	885.75	5.54	42.74
ZSL	ExCNet [24]	5.55	723.56	4.38	46.74
	Zero-DCE [25]	5.82	307.09	4.76	<b>46.85</b>
	RRDNet [26]	5.97	<b>142.89</b>	4.84	45.31

of Retinex-Net [4], KinD++ [54], and EnlightenGAN [23] is relatively better than the other methods. Retinex-Net [4] achieves the best PI and SPAQ scores. The scores suggest the good perceptual quality of the results enhanced by Retinex-Net [4]. However, from Fig. 7(d) and Fig. 8(d), the results of Retinex-Net [4] evidently suffer from artifacts and color deviations. Hence, we argue that the non-reference PI and SPAQ metrics may not be suitable for perceptual quality evaluation of low-light images. Moreover, KinD++ [54] attains the lowest NIQE score while the original input achieves the lowest LOE score. For the de-facto standard LOE metric, we question if the lightness order can effectively reflect the enhancement performance. Overall, the non-reference IQA metrics experience biases on the evaluations of the quality of enhanced low-light images.

To prepare videos in the LoLi-vidT testing set, we first discard videos without obvious objects in consecutive frames. A total of 10 videos are chosen. For each video, we select one object that appears in all frames. We then use a tracker [81] to track the object in consecutive frames of the input video and ensure the same object appear in



TABLE 7: Quantitative comparisons on LoLi-Phone-vidT dataset in terms of average luminance variance (ALV) score. The best result is in red whereas the second and third best results are in blue and purple.

Learning	Method	LoLi-Phone-vidT
		ALV↓
	input	185.60
SL	LLNet [1]	85.72
	LightenNet [5]	643.93
	Retinex-Net [4]	94.05
	MBLLEN [3]	113.18
	KinD [11]	98.05
	KinD++ [54]	115.21
	TBEFN [20]	58.69
	DSLRL [21]	175.35
UL	EnlightenGAN [23]	90.69
SSL	DRBN [27]	115.04
ZSL	ExCNet [24]	1375.29
	Zero-DCE [25]	117.22
	RRDNet [26]	147.11

the bounding boxes. We discard the frames with inaccurate object tracking. The coordinates of the bounding box in each frame are collected. We employ these coordinates to crop the corresponding regions in the results enhanced by different methods and compute the average luminance variance (ALV) scores of the object in the consecutive frames as:  $ALV = \frac{1}{N} \sum_{i=1}^N (L_i - L_{avg})^2$ , where  $N$  is the number of frames of a video,  $L_i$  represents the average luminance value of the region of bounding box in the  $i$ th frame, and  $L_{avg}$  denotes the average luminance value of all bounding box regions in the video. A lower ALV value suggests better temporal coherence of the enhanced video. The ALV values of different methods averaged over the 10 videos of LoLi-vidT testing set are shown in Table 7. The ALV values of different methods on each video can be found in the supplementary material. Besides, we follow [9] to plot their luminance curves in the supplementary material.

As shown in Table 7, TBEFN [20] obtains the best temporal coherence in terms of ALV value whereas LLNet [1] and EnlightenGAN [23] rank the second and third best, respectively. In contrast, the ALV value of ExCNet [24], as the worst performer, reaches 1375.29. This is because the performance of the zero-reference learning-based ExCNet [24] is unstable for the enhancement of consecutive frames. In other words, ExCNet [24] can effectively improve the brightness of some frames while it does not work well on other frames.

#### 4.4 Computational Complexity

In Table 8, we compare the computational complexity of different methods, including runtime, trainable parameters, and FLOPs averaged over 32 images of size  $1200 \times 900 \times 3$  using an NVIDIA 1080Ti GPU. We omit LightenNet [5] for fair comparisons because only the CPU version of its code is publicly available. Besides, we do not report the FLOPs of ExCNet [24] and RRDNet [26] because the number depends on the input images (different inputs require different numbers of iterations).

As presented in Table 8, Zero-DCE [25] has the shortest runtime because it only estimates several curve parameters

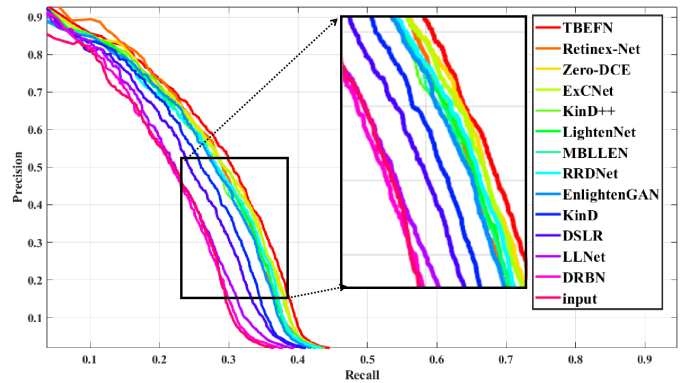


Fig. 9: The P-R curves of face detection in the dark.

via a lightweight network. As a result, its number of trainable parameters and FLOPs are much fewer. Moreover, the number of trainable parameters and FLOPs of LightenNet [5] are the least among the compared methods. This is because LightenNet [5] estimates the illumination map of input image via a tiny network of four convolutional layers. In contrast, the FLOPs of LLNet [1] and KinD++ [54] are extremely large, reaching 4124.177G and 12238.026G, respectively. The runtime of SSL-based ExCNet [24] and RRDNet [26] is long due to the time-consuming optimization process.

#### 4.5 Application-Based Evaluation

We investigate the performance of low-light image enhancement methods on face detection in the dark. Following the setting presented in [25], we use the DARK FACE dataset [73] that is composed of images with faces taken in the dark. Since the bounding boxes of test set are not publicly available, we perform the evaluation on 500 images randomly sampled from the training and validation sets. The Dual Shot Face Detector (DSFD) [82] trained on WIDER FACE dataset [83] is used as the face detector. We feed the results of different LLIE methods to the DSFD [82] and depict the precision-recall (P-R) curves under 0.5 IoU threshold in Figure 9. In addition, we compare the average precision (AP) under different IoU thresholds using the evaluation tool<sup>3</sup> provided in DARK FACE dataset [73] in Table 9.

As shown in Figure 9, all the deep learning-based solutions improve the performance of face detection in the dark, suggesting the effectiveness of deep learning-based LLIE solutions for face detection in the dark. As shown in Table 9, the AP scores of best performers under different IoU thresholds range from 0.268 to 0.013 and the AP scores of input under different IoU thresholds are very low. The results suggest that there are still rooms for improvement. It is noteworthy that Retinex-Net [4], Zero-DCE [25], and TBEFN [20] achieve relatively robust performance on face detection in the dark. We show the visual results of different methods in Figure 10. Although Retinex-Net [4] performs better than other methods on the AP score, its visual result contains obvious artifacts and unnatural textures. In general, Zero-DCE [25] obtains a good balance between the AP score and the perceptual quality for face detection in the dark.

3. [https://github.com/Ir1d/DARKFACE\\_eval\\_tools](https://github.com/Ir1d/DARKFACE_eval_tools)



TABLE 8: Quantitative comparisons of computational complexity in terms of runtime (in second), number of trainable parameters (#Parameters) (in M), and FLOPs (in G). The best result is in **red** whereas the second and third best results are in **blue** and **purple** under each case, respectively. ‘-’ indicates the result is not available.

Learning	Method	RunTime↓	#Parameters ↓	FLOPs↓	Platform
SL	LLNet [1]	36.270	17.908	4124.177	Theano
	LightenNet [5]	-	<b>0.030</b>	<b>30.540</b>	MATLAB
	Retinex-Net [4]	0.120	0.555	587.470	TensorFlow
	MBLLEN [3]	13.995	<b>0.450</b>	301.120	TensorFlow
	KinD [11]	0.148	8.160	574.954	TensorFlow
	KinD++ [54]	1.068	8.275	12238.026	TensorFlow
	TBEFN [20]	<b>0.050</b>	0.486	108.532	TensorFlow
UL	DSLRL [21]	0.074	14.931	<b>96.683</b>	PyTorch
	EnlightenGAN [23]	<b>0.008</b>	8.637	273.240	PyTorch
SSL	DRBN [27]	0.878	0.577	196.359	PyTorch
ZSL	ExCNet [24]	23.280	8.274	-	PyTorch
	Zero-DCE [25]	<b>0.003</b>	<b>0.079</b>	<b>84.990</b>	PyTorch
	RRDNet [26]	167.260	0.128	-	PyTorch



Fig. 10: Visual results of different methods on a low-light image sampled from DARK FACE dataset. Better see with zoom in for the bounding boxes of faces.

#### 4.6 Discussion

From the experimental results, we obtain several interesting observations and insights:

- The performance of different methods significantly varies based on the testing datasets and evaluation metrics. In terms of the full-reference IQA metrics on commonly used testing datasets, MBLLEN [3], KinD++ [54], and DSLR [21] are generally better than other compared methods. For real-world low-light images taken by mobile phones, supervised learning-based Retinex-Net [4] and KinD++ [54] obtain better scores measured in the non-reference IQA metrics. For real-world low-light videos taken by

mobile phones, TBEFN [20] preserves the temporal coherence better. When coming to the computational efficiency, LightenNet [5] and Zero-DCE [25] are outstanding. From the aspect of face detection in the dark, TBEFN [20], Retinex-Net [4], and Zero-DCE [25] rank the first three. No method always wins. Overall, Retinex-Net [4], [20], Zero-DCE [25], and DSLR [21] are better choice in most cases.

- Low-light images and videos of the proposed LoLi-Phone dataset fail most methods. The generalization capability of existing methods needs further improvements. It is worth noting that it is inadequate to use only the average luminance variance to evaluate the performance of different methods for low-light

TABLE 9: Quantitative comparisons of AP under different IoU thresholds of face detection in the dark. The best result is in red whereas the second and third best results are in blue and purple under each case, respectively.

Learning	Method	IoU thresholds		
		0.5	0.6	0.7
	input	0.195	0.061	0.007
SL	LLNet [1]	0.208	0.063	0.006
	LightenNet [5]	0.249	0.085	0.010
	Retinex-Net [4]	0.261	0.101	0.013
	MBLLEN [3]	0.249	0.092	0.010
	KinD [11]	0.235	0.081	0.010
	KinD++ [54]	0.251	0.090	0.011
	TBEFN [20]	0.268	0.099	0.011
	DSLRL [21]	0.223	0.067	0.007
UL	EnlightenGAN [23]	0.246	0.088	0.011
SSL	DRBN [27]	0.199	0.061	0.007
ZSL	ExCNet [24]	0.256	0.092	0.010
	Zero-DCE [25]	0.259	0.092	0.011
	RRDNet [26]	0.248	0.083	0.010

video enhancement. More effective and comprehensive assessment metrics would guide the development of low-light video enhancement towards the right track.

- Regarding learning strategies, supervised learning achieves better performance in most cases, but requires high computational resources and paired training data. In comparison, zero-shot learning is more appealing in practical applications because it does not require paired or unpaired training data. Consequently, zero-shot learning-based methods enjoy better generalization capability. However, quantitative performance of zero-shot learning-based methods is inferior to other methods.
- There is a gap between visual results and quantitative IQA scores. In other words, a good visual appearance does not always yield a good IQA score. The relations between human perception and IQA scores are worth more investigations. Pursuing better visual perception or quantitative scores depends on specific applications. For instance, to show the results to observers, more attention should be paid to the visual perception. In contrast, the accuracy is more important than the visual perception when LLIE methods are applied to face detection in the dark. Thus, more comprehensive and thorough comparisons should be performed when comparing different methods.
- Deep learning-based LLIE methods are beneficial to face detection in the dark. Such results further support the significance of enhancing low-light images and videos. However, in comparison to the high accuracy of face detection in the image of normal light, the accuracy of face detection in the dark is extremely low, in spite of using LLIE methods.

## 5 FUTURE RESEARCH DIRECTIONS

Low-light image enhancement is a challenging research topic. As can be observed from the experiments presented in

Section 4, there are still rooms for improvement. We suggest potential future research directions as follows.

**Effective Learning Strategies.** As aforementioned, current LLIE models mainly adopt supervised learning that requires massive paired training data and may overfit on a specific dataset. Although some researchers attempted to introduce unsupervised learning, e.g., adversarial learning, into LLIE, the inherent relations between LLIE and these learning strategies are not clear and their effectiveness in LLIE needs further improvements. Zero-shot learning has shown robust performance for real scenes while not requiring paired training data. The unique advantage suggests zero-shot learning as a potential research direction, especially on the formulation of zero-reference losses, deep priors, and optimization strategies.

**Specialized Network Structures.** A network structure can significantly affect the enhancement performance. As previously analyzed, most LLIE deep models employ a U-Net or U-Net-like structures. Though they have achieved promising performance in some cases, the investigation if such an encoder-decoder network structure is most suitable for LLIE task is still lacking. Some network structures require a high memory footprint and long inference time due to their large parameter space. Such network structures are unacceptable for practical applications. Thus, it is worthwhile to investigate a more effective network structure for LLIE, considering the characteristics of low-light images such as non-uniform illumination, small pixel values, noise suppression, and color constancy. One can also design more efficient network structures via taking into account the local similarity of low-light images or considering more efficient operations such as depthwise separable convolution layer [84] and self-calibrated convolution [85]. Neural architecture search (NAS) technique [86], [87] may be considered to obtain more effective and efficient LLIE network structures. Adapting the transformer architecture [88], [89] into LLIE may be a potential and interesting research direction.

**Loss Functions.** Loss functions constrain the relations between input image and ground truth, and drive the optimization of deep networks. In LLIE, the commonly used loss functions are borrowed from related vision tasks. There is no specialized loss function for guiding the optimization of low-light video enhancement networks. Thus, designing loss functions that are more well-suited for LLIE is desired. In addition, recent studies have shown the possibility of using deep neural networks to approximate human visual perception of image quality [90], [91]. These ideas and fundamental theories could be used to guide the designs of appropriate loss function for low-light enhancement networks.

**Realistic Training Data.** Although there are several training datasets for LLIE, their authenticity, scales, and diversities fall behind real low-light conditions. Thus, as shown in Section 4, current LLIE deep models cannot achieve satisfactory performance when encountering low-light images captured in real-world scenes. More efforts are needed to study the collection of large-scale and diverse real-world paired LLIE training datasets or to generate more realistic synthetic data. **Standard Testing Data.** Currently, there is no well-accepted LLIE evaluation benchmark. Researchers prefer selecting their own testing data that may bias to their proposed meth-

ods. Despite some researchers leave some paired data as test data, the division of training and test partitions are mostly ad-hoc across the literature. Consequently, conducting a fair comparison among different methods is often laborious if not impossible. Besides, some test data are either easy to be handled or not originally collected for low-light enhancement. It is desired to have a standard low-light image and video test dataset, which includes a large quantity of test samples with the corresponding ground truths, covering diverse scenes and challenging illumination conditions.

**Task-Specific Evaluation Metrics.** The commonly adopted evaluation metrics in LLIE can reflect the image quality to some extent. However, how to measure how good a result is enhanced by a LLIE method still challenges current IQA metrics, especially for non-reference measurements. Moreover, the current IQA metrics either focus on human visual perceptual such as subjective quality or emphasize machine perceptual such as the effects on high-level visual tasks. An evaluation metric that takes both human perceptual and machine perceptual into account is desired. Therefore, more works are expected in this research direction to make efforts on designing more accurate and task-specific evaluation metrics for LLIE.

**Robust Generalization Capability.** Observing the experimental results on real-world test data, most methods fail due to their limited generalization capability. The poor generalization is caused by several factors such as synthetic training data, small-scaled training data, ineffective network structures, unrealistic assumptions, and inaccurate priors. It is important to explore ways to improve the generalization of deep learning-based LLIE models.

**Extension to Low-Light Video Enhancement.** Unlike the rapid development of video enhancement in other low-level vision tasks such as video deblurring [92], video denoising [93], and video super-resolution [94], low-light video enhancement receives less attention. A direct application of existing LLIE methods to videos often lead to unsatisfactory results and flickering artifacts. More efforts are needed to remove visual flickering effectively, exploit the temporal information between neighboring frames, and speed up the enhancement speed.

**Integrating Semantic Information.** Semantic information is crucial for low-light enhancement. It guides the networks to distinguish different regions in the process of enhancement. A network without the access to semantic priors can easily deviate the original color of a region, e.g., turning black hair to gray color after enhancement. Therefore, integrating semantic priors into LLIE models is a promising research direction. Similar work has been done on image super-resolution [95], [96] and face restoration [97].

## REFERENCES

- [1] K. G. Lore, A. Akintayo, and S. Sarkar, "LLNet: A deep autoencoder approach to natural low-light image enhancement," *Pattern Recognition*, vol. 61, pp. 650–662, 2017.
- [2] C. Chen, Q. Chen, J. Xu, and V. Koltun, "Learning to see in the dark," in *Proceedings of the IEEE Conference on Computer Vision and Pattern Recognition*, 2018, pp. 3291–3300.
- [3] F. Lv, F. Lu, J. Wu, and C. Lim, "MBLLEN: Low-light image/video enhancement using cnns," in *Proceedings of the British Machine Vision Conference*, 2018.
- [4] C. Wei, W. Wang, W. Yang, and J. Liu, "Deep retinex decomposition for low-light enhancement," in *Proceedings of the British Machine Vision Conference*, 2018.
- [5] C. Li, J. Guo, F. Porikli, and Y. Pang, "LightenNet: A convolutional neural network for weakly illuminated image enhancement," *Pattern Recognition Letters*, vol. 104, pp. 15–22, 2018.
- [6] J. Cai, S. Gu, and L. Zhang, "Learning a deep single image contrast enhancer from multi-exposure images," *IEEE Transactions on Image Processing*, vol. 27, no. 4, pp. 2049–2062, 2018.
- [7] R. Wang, Q. Zhang, C.-W. Fu, X. Shen, W.-S. Zheng, and J. Jia, "Underexposed photo enhancement using deep illumination estimation," in *Proceedings of the IEEE Conference on Computer Vision and Pattern Recognition*, 2019, pp. 6849–6857.
- [8] C. Chen, Q. Chen, M. N. Do, and V. Koltun, "Seeing motion in the dark," in *Proceedings of the International Conference on Computer Vision*, 2019, pp. 3185–3194.
- [9] H. Jiang and Y. Zheng, "Learning to see moving object in the dark," in *Proceedings of the International Conference on Computer Vision*, 2019, pp. 7324–7333.
- [10] Y. Wang, Y. Cao, Z. Zha, J. Zhang, Z. Xiong, W. Zhang, and F. Wu, "Progressive retinex: Mutually reinforced illumination-noise perception network for low-light image enhancement," in *Proceedings of the ACM International Conference on Multimedia*, 2019, pp. 2015–2023.
- [11] Y. Zhang, J. Zhang, and X. Guo, "Kindling the darkness: A practical low-light image enhancer," in *Proceedings of the ACM International Conference on Multimedia*, 2019, pp. 1632–1640.
- [12] W. Ren, S. Liu, L. Ma, Q. Xu, X. Xu, X. Cao, J. Du, and M.-H. Yang, "Low-light image enhancement via a deep hybrid network," *IEEE Transactions on Image Processing*, vol. 28, no. 9, pp. 4364–4375, 2019.
- [13] K. Xu, X. Yang, B. Yin, and R. W. H. Lau, "Learning to restore low-light images via decomposition-and-enhancement," in *Proceedings of the IEEE Conference on Computer Vision and Pattern Recognition*, 2020, pp. 2281–2290.
- [14] M. Fan, W. Wang, W. Yang, and J. Liu, "Integrating semantic segmentation and retinex model for low light image enhancement," in *Proceedings of the ACM International Conference on Multimedia*, 2020, pp. 2317–2325.
- [15] F. Lv, B. Liu, and F. Lu, "Fast enhancement for non-uniform illumination images using light-weight cnns," in *Proceedings of the ACM International Conference on Multimedia*, 2020, pp. 1450–1458.
- [16] M. Zhu, P. Pan, W. Chen, and Y. Yang, "EEMEFN: Low-light image enhancement via edge-enhanced multi-exposure fusion network," in *Proceedings of the Association for the Advancement of Artificial Intelligence*, 2020, pp. 13 106–13 113.
- [17] D. Triantafyllidou, S. Moran, S. McDonagh, S. Parisot, and G. Slabaugh, "Low light video enhancement using synthetic data produced with an intermediate domain mapping," in *Proceedings of the European Conference on Computer Vision*, 2020, pp. 103–119.
- [18] J. Li, J. Li, F. Fang, F. Li, and G. Zhang, "Luminance-aware pyramid network for low-light image enhancement," *IEEE Transactions on Multimedia*, 2020.
- [19] L. Wang, Z. Liu, W. Siu, and D. P. K. Lun, "Lightening network for low-light image enhancement," *IEEE Transactions on Image Processing*, vol. 29, pp. 7984–7996, 2020.
- [20] K. Lu and L. Zhang, "TBEFN: A two-branch exposure-fusion network for low-light image enhancement," *IEEE Transactions on Multimedia*, 2020.
- [21] S. Lim and W. Kim, "DSLRL: Deep stacked laplacian restorer for low-light image enhancement," *IEEE Transactions on Multimedia*, 2020.
- [22] R. Yu, W. Liu, Y. Zhang, Z. Qu, D. Zhao, and B. Zhang, "DeepExposure: Learning to expose photos with asynchronously reinforced adversarial learning," in *Advances in Neural Information Processing Systems*, 2018, pp. 2149–2159.
- [23] Y. Jiang, X. Gong, D. Liu, Y. Cheng, C. Fang, X. Shen, J. Yang, P. Zhou, and Z. Wang, "EnlightenGAN: Deep light enhancement without paired supervision," *IEEE Transactions on Image Processing*, vol. 30, pp. 2340–2349, 2021.
- [24] L. Zhang, L. Zhang, X. Liu, Y. Shen, S. Zhang, and S. Zhao, "Zero-shot restoration of back-lit images using deep internal learning," in *Proceedings of the ACM International Conference on Multimedia*, 2019, pp. 1623–1631.
- [25] C. Guo, C. Li, J. Guo, C. C. Loy, J. Hou, S. Kwong, and R. Cong, "Zero-reference deep curve estimation for low-light image enhancement," in *Proceedings of the IEEE Conference on Computer Vision and Pattern Recognition*, 2020, pp. 1780–1789.



- [26] A. Zhu, L. Zhang, Y. Shen, Y. Ma, S. Zhao, and Y. Zhou, "Zero-shot restoration of underexposed images via robust retinex decomposition," in *Proceedings of the IEEE International Conference on Multimedia and Expo*, 2020, pp. 1–6.
- [27] W. Yang, S. Wang, Y. Fang, Y. Wang, and J. Liu, "From fidelity to perceptual quality: A semi-supervised approach for low-light image enhancement," in *Proceedings of the IEEE Conference on Computer Vision and Pattern Recognition*, 2020, pp. 3063–3072.
- [28] H. Ibrahim and N. S. P. Kong, "Brightness preserving dynamic histogram equalization for image contrast enhancement," *IEEE Transactions on Consumer Electronics*, vol. 53, no. 4, pp. 1752–1758, 2007.
- [29] M. Abdullah-AI-Wadud, M. H. Kabir, M. A. A. Dewan, and O. Chae, "A dynamic histogram equalization for image contrast enhancement," *IEEE Transactions on Consumer Electronics*, vol. 53, no. 2, pp. 593–600, 2007.
- [30] S. Wang, J. Zheng, H. Hu, and B. Li, "Naturalness preserved enhancement algorithm for non-uniform illumination images," *IEEE Transactions on Image Processing*, vol. 22, no. 9, pp. 3538–3548, 2013.
- [31] X. Fu, Y. Liao, D. Zeng, Y. Huang, X. Zhang, and X. Ding, "A probabilistic method for image enhancement with simultaneous illumination and reflectance estimation," *IEEE Transactions on Image Processing*, vol. 24, no. 12, pp. 4965–4977, 2015.
- [32] X. Guo, Y. Li, and H. Ling, "LIME: Low-light image enhancement via illumination map estimation," *IEEE Transactions on Image Processing*, vol. 26, no. 2, pp. 982–993, 2016.
- [33] S. Park, S. Yu, B. Moon, S. Ko, and J. Paik, "Low-light image enhancement using variational optimization-based retinex model," *IEEE Transactions on Consumer Electronics*, vol. 63, no. 2, pp. 178–184, 2017.
- [34] M. Li, J. Liu, W. Yang, X. Sun, and Z. Guo, "Structure-revealing low-light image enhancement via robust retinex model," *IEEE Transactions on Image Processing*, vol. 27, no. 6, pp. 2828–2841, 2018.
- [35] Z. Gu, F. Li, F. Fang, and G. Zhang, "A novel retinex-based fractional-order variational model for images with severely low light," *IEEE Transactions on Image Processing*, vol. 29, pp. 3239–3253, 2019.
- [36] X. Ren, W. Yang, W.-H. Cheng, and J. Liu, "LR3M: Robust low-light enhancement via low-rank regularized retinex model," *IEEE Transactions on Image Processing*, vol. 29, pp. 5862–5876, 2020.
- [37] S. Hao, X. Han, Y. Guo, X. Xu, and M. Wang, "Low-light image enhancement with semi-decoupled decomposition," *IEEE Transactions on Multimedia*, vol. 22, no. 12, pp. 3025–3038, 2020.
- [38] Y. Hu, H. He, C. Xu, B. Wang, and S. Lin, "Exposure: A white-box photo post-processing framework," *ACM Transactions on Graphics*, vol. 37, no. 2, pp. 1–17, 2018.
- [39] M. Gharbi, J. Chen, J. T. Barron, S. W. Hasinoff, and F. Durand, "Deep bilateral learning for real-time image enhancement," *ACM Transactions on Graphics*, vol. 36, no. 4, pp. 1–12, 2017.
- [40] Y. Chen, Y. Wang, M. Kao, and Y. Chuang, "Deep photo enhancer: Unpaired learning for image enhancement form photographs wigh gans," in *Proceedings of the IEEE Conference on Computer Vision and Pattern Recognition*, 2018, pp. 6306–6314.
- [41] Y. Deng, C. C. Loy, and X. Tang, "Aesthetic-driven image enhancement by adversarial learning," in *Proceedings of the ACM International Conference on Multimedia*, 2018, pp. 870–878.
- [42] Z. Yan, H. Zhang, B. Wang, S. Paris, and Y. Yu, "Automatic photo adjustment using deep neural networks," *ACM Transactions on Graphics*, vol. 35, no. 2, pp. 1–15, 2016.
- [43] Q. Chen, J. Xu, and V. Koltun, "Fast image processing with fully-convolutional networks," in *Proceedings of the IEEE Conference on Computer Vision and Pattern Recognition*, 2017, pp. 2497–2506.
- [44] Z. Ni, W. Yang, S. Wang, L. Ma, and S. Kwong, "Towards unsupervised deep image enhancement with generative adversarial network," *IEEE Transactions on Image Processing*, vol. 29, pp. 9140–9151, 2020.
- [45] H. Zeng, J. Cai, L. Li, Z. Cao, and L. Zhang, "Learning image-adaptive 3D lookup tables for high performance photo enhancement in real-time," *IEEE Transactions on Pattern Analysis and Machine Intelligence*, 2020.
- [46] C. Li, C. Guo, Q. Ai, S. Zhou, and C. C. Loy, "Flexible piecewise curves estimation for photo enhancement," *arXiv preprint arXiv:2010.13412*, 2020.
- [47] W. Wang, X. Wu, X. Yuan, and Z. Gao, "An experiment-based review of low-light image enhancement methods," *IEEE Access*, vol. 8, pp. 87 884–87 917, 2020.
- [48] J. Liu, D. Xu, W. Yang, M. Fan, and H. Huang, "Benchmarking low-light image enhancement and beyond," *International Journal of Computer Vision*, 2021.
- [49] V. Jain and S. Seung, "Natural image denoising with convolutional networks," in *Advances in Neural Information Processing Systems*, 2008, pp. 1–8.
- [50] K. Xu, X. Yang, B. Yin, and R. W. H. Lau, "Learning to restore low-light images via decomposition-and-enhancement," in *Proceedings of the IEEE Conference on Computer Vision and Pattern Recognition*, 2020, pp. 2281–2290.
- [51] E. H. Land, "An alternative technique for the computation of the designator in the retinex theory of color vision," *Proceedings of the National Academy of Sciences*, vol. 83, no. 10, pp. 3078–3080, 1986.
- [52] D. J. Jobson, Z. ur Rahman, and G. A. Woodell, "Properties and performance of a center/surround retinex," *IEEE Transactions on Image Processing*, vol. 6, no. 3, pp. 451–462, 1997.
- [53] R. Wang, Q. Zhang, C.-W. Fu, X. Shen, W.-S. Zheng, and J. Jia, "Underexposed photo enhancement using deep illumination estimation," in *Proceedings of the IEEE Conference on Computer Vision and Pattern Recognition*, 2019, pp. 6849–6857.
- [54] X. Guo, Y. Zhang, J. Ma, W. Liu, and J. Zhang, "Beyond brightening low-light images," *International Journal of Computer Vision*, 2020.
- [55] O. Ronneberger, P. Fischer, and T. Brox, "U-Net: Convolutional networks for biomedical image segmentation," in *Proceedings of International Conference on Medical Image Computing and Computer Assisted Intervention*, 2015, pp. 234–241.
- [56] T. Xue, B. Chen, J. Wu, D. Wei, and W. T. Freeman, "Video enhancement with task-oriented flow," *International Journal of Computer Vision*, vol. 127, no. 8, pp. 1106–1125, 2019.
- [57] K. He, J. Sun, and X. Tang, "Guided image filtering," *IEEE Transactions on Pattern Analysis and Machine Intelligence*, vol. 35, no. 6, pp. 1397–1409, 2013.
- [58] P. Whittle, "The psychophysics of contrast brightness," A. L. Gilchrist (Ed.), *Brightness, lightness, and transparenc* (1994), pp. 35–110, 1993.
- [59] C. Li, C. Guo, and C. C. Loy, "Learning to enhance low-light image via zero-reference deep curve estimation," *IEEE Trans. Pattern Anal. Mach. Intell.*, 2021.
- [60] Z. Wang, A. C. Bovik, H. R. Sheikh, and E. P. Simoncelli, "Image quality assessment: From error visibility to structural similarity," *IEEE Transactions on Image Processing*, vol. 13, no. 4, pp. 600–612, 2004.
- [61] H. Zhao, O. Gallo, I. Frosio, and J. Kautz, "Loss functions for image restoration with neural networks," *IEEE Transactions on Image Processing*, vol. 3, no. 1, pp. 47–56, 2017.
- [62] C. Ledig, L. Theis, F. Huszar, J. Caballero, A. Cunningham, A. Acosta, A. Aitken, A. Tejani, J. Totz, Z. Wang, and W. Shi, "Photo-realistic single image super-resolution using a generative adversarial network," in *Proceedings of the IEEE Conference on Computer Vision and Pattern Recognition*, 2017, pp. 4681–4690.
- [63] K. Simoayan and A. Zisserman, "Very deep convolutional networks for large-scale image recognition," *arXiv preprint arXiv:1409.1556*, 2014.
- [64] J. Deng, W. Dong, R. Socher, L. Li, K. Li, and L. Fei-Fei, "ImageNet: A large-scale hierarchical image database," in *Proceedings of the IEEE Conference on Computer Vision and Pattern Recognition*, 2009, pp. 248–255.
- [65] C. Dong, C. C. Loy, K. He, and X. Tang, "Image super-resolution using deep convolutional networks," *IEEE Transactions on Pattern Analysis and Machine Intelligence*, vol. 38, no. 2, pp. 295–307, 2015.
- [66] Q. Xu, C. Zhang, and L. Zhang, "Denoising convolutional neural network," in *Proceedings of the IEEE International Conference on Information and Automation*, 2015, pp. 1184–1187.
- [67] X. Fu, J. Huang, D. Zeng, Y. Huang, X. Ding, and J. Paisley, "Removing rain from single images via a deep detail network," in *Proceedings of the IEEE Conference on Computer Vision and Pattern Recognition*, 2017, pp. 3855–3863.
- [68] W. Yang, R. T. Tan, J. Feng, J. Liu, Z. Guo, and S. Yan, "Deep joint rain detection and removal from a single image," in *Proceedings of the IEEE Conference on Computer Vision and Pattern Recognition*, 2017, pp. 1357–1366.
- [69] J. Sun, W. Cao, Z. Xu, and J. Ponce, "Learning a convolutional neural network for non-uniform motion blur removal," in *Proceedings of the IEEE Conference on Computer Vision and Pattern Recognition*, 2015, pp. 769–777.
- [70] V. Bychkovsky, S. Paris, E. Chan, and F. Durand, "Learning photographic global tonal adjustment with a database of input/output

- image pairs,” in *Proceedings of the IEEE Conference on Computer Vision and Pattern Recognition*, 2011, pp. 97–104.
- [71] L. Chulwoo, L. Chul, L. Young-Yoon, and K. Chang-su, “Power-constrained contrast enhancement for emissive displays based on histogram equalization,” *IEEE Transactions on Image Processing*, vol. 21, no. 1, pp. 80–93, 2012.
- [72] C. Lee, C. Lee, and C.-S. Kim, “Contrast enhancement based on layered difference representation of 2d histograms,” *IEEE Transactions on Image Processing*, vol. 22, no. 12, pp. 5372–5384, 2013.
- [73] Y. Yuan, W. Yang, W. Ren, J. Liu, W. JScheirer, and W. Zhangyang, “UG+ Track 2: A collective benchmark effort for evaluating and advancing image understanding in poor visibility environments,” *arXiv arXiv:1904.04474*, 2019.
- [74] Y. P. Loh and C. S. Chan, “Getting to know low-light images with the exclusively dark dataset,” *Computer Vision and Image Understanding*, vol. 178, pp. 30–42, 2019.
- [75] F. Yu, W. Xian, Y. Chen, F. Liu, M. Liao, V. Madhavan, and T. Darrell, “BDD100K: A diverse driving video database with scalable annotation tooling,” *arXiv preprint arXiv:1805.04687*, 2018.
- [76] R. Zhang, P. Isola, A. A. Efros, E. Shechtman, and O. Wang, “The unreasonable effectiveness of deep features as a perceptual metric,” in *Proceedings of the IEEE Conference on Computer Vision and Pattern Recognition*, 2018, pp. 586–595.
- [77] A. Mittal, R. Soundararajan, and A. C. Bovik, “Making a completely blind image quality analyzer,” *IEEE Signal Processing Letters*, vol. 20, no. 3, pp. 209–212, 2013.
- [78] Y. Blau and T. Michaeli, “The perception-distortion tradeoff,” in *Proceedings of the IEEE Conference on Computer Vision and Pattern Recognition*, 2018, pp. 6228–6237.
- [79] C. Ma, C.-Y. Yang, X. Yang, and M.-H. Yang, “Learning a non-reference quality metric for single-image super-resolution,” *Computer Vision and Image Understanding*, vol. 158, pp. 1–16, 2017.
- [80] Y. Fang, H. Zhu, Y. Zeng, K. Ma, and Z. Wang, “Perceptual quality assessment of smartphone photography,” in *Proceedings of the International Conference on Computer Vision*, 2020, pp. 3677–3686.
- [81] M. Danelljan, G. Bhat, F. S. Khan, and M. Felsberg, “ECO: Efficient convolution operators for tracking,” in *Proceedings of the IEEE Conference on Computer Vision and Pattern Recognition*, 2017, pp. 6638–6646.
- [82] J. Li, Y. Wang, C. Wang, Y. Tai, J. Qian, J. Yang, C. Wang, J. Li, and F. Huang, “DSFD: Dual shot face detector,” in *Proceedings of the IEEE Conference on Computer Vision and Pattern Recognition*, 2019, pp. 5060–5069.
- [83] S. Yang, P. Luo, C. C. Loy, and X. Tang, “Wider Face: A face detection benchmark,” in *Proceedings of the IEEE Conference on Computer Vision and Pattern Recognition*, 2016, pp. 5525–5533.
- [84] A. G. Howard, M. Zhu, B. Chen, D. Kalenichenko, W. Wang, T. Weyand, M. Andreetto, and H. Adam, “MobileNets: Efficient convolutional neural networks for mobile vision application,” *arXiv preprint arXiv:1704.04861*, 2017.
- [85] J. Liu, Q. Hou, M. M. Cheng, C. Wang, and J. Feng, “Improving convolutional networks with self-calibrated convolutions,” in *Proceedings of the IEEE Conference on Computer Vision and Pattern Recognition*, 2020, pp. 10 096–10 105.
- [86] C. Liu, B. Zoph, M. Neumann, J. Shlens, W. Hua, L. Li, L. F. Fei, A. Yuille, J. Huang, and K. Murphy, “Progressive neural architecture search,” in *Proceedings of the European Conference on Computer Vision*, 2018, pp. 19–34.
- [87] C. Liu, L. C. Chen, F. Schroff, H. Adam, W. Hua, A. Yuille, and L. F. Fei, “Auto-Deeplab: Hierarchical neural architecture search for semantic image segmentation,” in *Proceedings of the IEEE Conference on Computer Vision and Pattern Recognition*, 2019, pp. 82–92.
- [88] A. Dosovitskiy, L. Beyer, A. Kolesnikov, D. Weissenborn, X. Zhai, T. Unterthiner, M. D. M. Minderer, G. Heigold, S. Gelly, J. Uszkoreit, and N. Houlsby, “An image is worth 16x16 words: Transformers for image recognition at scale,” *arXiv preprint arXiv:2010.11929*, 2020.
- [89] H. Chen, Y. Wang, T. Guo, C. Xu, Y. Deng, Z. Liu, S. Ma, C. Xu, C. Xu, and W. Gao, “Pre-trained image processing transformer,” *arXiv preprint arXiv:2012.00364*, 2020.
- [90] Y. Fang, H. Zhu, Y. Zeng, K. Ma, and Z. Wang, “Perceptual quality assessment of smartphone photography,” in *Proceedings of the IEEE Conference on Computer Vision and Pattern Recognition*, 2020, pp. 3677–3686.
- [91] H. Talebi and P. Milanfar, “NIMA: Neural image assessment,” *IEEE Transactions on Image Processing*, vol. 27, no. 8, pp. 3998–4011, 2018.
- [92] T. H. Kim, K. M. Lee, B. Scholkopf, and M. Hirsch, “Online video deblurring via dynamic temporal blending network,” in *Proceedings of the International Conference on Computer Vision*, 2017, pp. 4038–4047.
- [93] T. Ehret, A. Davy, J.-M. Morel, G. Facciolo, and P. Arias, “Model-blind video denoising via frame-to-frame training,” in *Proceedings of the IEEE Conference on Computer Vision and Pattern Recognition*, 2019, pp. 11 369–11 378.
- [94] K. C. K. Chan, X. Wang, K. Yu, C. Dong, and C. C. Loy, “BasicVSR: The search for essential components in video super-resolution and beyond,” in *Proceedings of the IEEE Conference on Computer Vision and Pattern Recognition*, 2021.
- [95] X. Wang, K. Yu, C. Dong, and C. C. Loy, “Recovering realistic texture in image super-resolution by deep spatial feature transform,” in *Proceedings of the IEEE Conference on Computer Vision and Pattern Recognition*, 2018, pp. 606–615.
- [96] K. C. K. Chan, X. Wang, X. Xu, J. Gu, and C. C. Loy, “GLEAN: Generative latent bank for large-factor image super-resolution,” in *Proceedings of the IEEE Conference on Computer Vision and Pattern Recognition*, 2021.
- [97] X. Li, C. Chen, S. Zhou, X. Lin, W. Zuo, and L. Zhang, “Blind face restoration via deep multi-scale component dictionaries,” in *Proceedings of the European Conference on Computer Vision*, 2020, pp. 399–415.